THE ASTROPHYSICAL JOURNAL, 536:195–212, 2000 June 10

WIND INTERACTION MODELS FOR GAMMA-RAY BURST AFTERGLOWS: THE CASE FOR TWO TYPES OF PROGENITORS

ROGER A. CHEVALIER AND ZHI-YUN LI
Department of Astronomy, University of Virginia, P.O. Box 3818, Charlottesville, VA 22903; rac5x@virginia.edu, zl4h@virginia.edu
Received 1999 August 24; accepted 2000 January 26

ABSTRACT

Beginning with the γ-ray bursts GRB 970228 and GRB 970508, a standard model for the interpretation of gamma-ray burst (GRB) afterglows emerged involving synchrotron emission from a constant-energy blast wave expanding into a constant-density, "interstellar" medium. However, a massive star origin for GRBs implies a stellar wind environment, probably a Wolf-Rayet star, and we have previously suggested wind interaction models for the afterglows of GRBs 980326, 980519, and 980425/SN 1998bw. Here, we extend the theory of afterglows in winds, considering strong cooling phases, the transition to nonrelativistic motion, jets, and prompt reverse-shock emission. We find that, compared to the interstellar case, the optical prompt emission in the wind case could have a comparable magnitude but would die off faster. We examine the afterglows of other well-observed GRBs in the context of wind interaction models and find that GRBs 970228 and 970508 are likely wind interactors. The revision in the nonthermal afterglow emission from GRB 970228 caused by the recognition of late supernova emission favors wind interaction. The radio evolution of GRB 970508 provides especially strong evidence for wind interaction. For GRB 970508, the observations suggest a density that is compatible with that expected in a Wolf-Rayet star wind. Finally, observations of the afterglow evolution of GRBs 990123 and 990510 and the prompt optical emission from GRB 990123 favor interstellar interaction models, which would suggest compact star merger progenitors for these objects.

Subject headings: gamma rays: bursts — stars: mass loss — supernovae: general

1. INTRODUCTION

The fireball model for gamma-ray bursts (GRBs) led to predictions of the afterglow emission that might be expected when the energetic shock wave encountered the surrounding medium (Katz 1994; Mészáros & Rees 1997). The subsequent optical and X-ray observations of the afterglow from GRB 970228 appeared to confirm the predictions of the simplest afterglow model (Waxman 1997a; Wijers, Rees, & Mészáros 1997). This model involved synchrotron emission from electrons accelerated to a power-law energy spectrum in a relativistic blast wave expanding into a constant-density, presumably interstellar medium (ISM). In particular, the expected relation between the flux spectral index and the power-law rate of flux decay was in approximate accord with the observations. This model has become the "standard model" for the interpretation of GRB afterglow observations. It was used to make predictions of bright optical emission in the early phases when a reverse-shock front is present (Sari & Piran 1999b). The observation of a bright flash from GRB 990123 (Akerlof et al. 1999) gave basic confirmation of this aspect of the model (Sari & Piran 1999a; Mészáros & Rees 1999). The expectation of jets for the initial energy deposition led to predictions of the effects on the light curve as the jet slowed (Rhoads 1997, 1999; Sari, Piran, & Halpern 1999). The observations of the afterglow of GRB 990510 confirmed the basic features expected for jet deceleration (Harrison et al. 1999).

These successes of the standard model give confidence that it is essentially correct. However, there has been increasing evidence that at least some GRBs have massive star progenitors, as initially suggested by Woosley (1993) on theoretical grounds. Paczyński (1998) noted that the available evidence on the location of GRBs in their host galaxies indicated a link to star formation. A more direct link to massive stars is provided by the presence of a supernova, the light from the exploded star matter. GRB 980425 was probably associated with the relatively nearby Type Ic supernova SN 1998bw (Galama et al. 1998d; Kulkarni et al. 1998), and evidence for supernova-type emission has now been found in GRB 980326 (Bloom et al. 1999b) and GRB 970228 (Reichart 1999; Galama et al. 2000).

The importance of a massive star origin for the afterglow evolution is that the GRB blast wave should be expanding into the stellar wind of the progenitor star. Dai & Lu (1998), Mészáros, Rees, & Wijers (1998), and Panaitescu, Mészáros, & Rees (1998) described some features of afterglow evolution in a $\rho \propto r^{-2}$ stellar wind. Chevalier & Li (1999, hereafter CL) made specific estimates for expansion into the wind of a Wolf-Rayet star. Li & Chevalier (1999) and CL identified GRB 980425/SN 1998bw, GRB 980326, and GRB 980519 as likely circumstellar wind interactors based on their afterglow evolution. In the cases of GRB 980425 and 980326, this association is supported by the presence of supernova emission. In GRB 980519, a supernova would have to be somewhat fainter than SN 1998bw (Bloom 1999). CL identified GRB 990123 as a likely interstellar interactor based on its afterglow evolution. GRBs of this type are not expected to be accompanied by supernovae.

CL placed the afterglows of GRB 980519 and GRB 980326 in the wind category partly based on their relatively rapid rates of decline of optical emission. An alternative explanation for the decline is that the emission is from a laterally expanding jet (Sari et al. 1999; Halpern et al. 1999). However, in the case of GRB 980519, CL were able to use radio observations made during the first 3 days (Frail et al. 1998b) to constrain the model further and to predict the radio evolution. Radio data on GRB 980519 over the first 63 days are now available (Frail et al. 2000b), and they are in agreement with the prediction of CL. The jet model does

not appear to fit the data as well, but scintillation effects cause sufficiently large uncertainties in the radio fluxes that the jet model is also acceptable.

In view of the increasing evidence for massive star progenitors of GRBs, our aim here is to develop the theory of wind interaction further and to examine the data on afterglows in the context of wind and interstellar interaction models. In § 2, we extend the theory of afterglows in winds to consider strong cooling, nonrelativistic evolution, and jets. Our discussion is guided by previous discussions of the constant-density interaction case, and we contrast the two situations. The differences are expected to be especially significant for prompt emission because of the large difference in the ambient density at early times. We treat prompt, reverse-shock emission for the wind case in § 3. In § 4, we examine the data on the best observed afterglows in the context of the wind and constant-density models. We find that wind models can explain a number of observations previously regarded as puzzling, pointing to wind interaction models for these cases. Although wind models are indicated for some observed afterglows, there are others that are better described by constant-density interaction. We discuss some implications of this result in § 5. Our conclusions are listed in § 6.

2. AFTERGLOW LIGHT CURVES IN WINDS

2.1. *Blast-Wave Hydrodynamics*

The basic model for GRB afterglow hydrodynamics involves a relativistic blast wave expanding into the surrounding medium (e.g., Mészáros & Rees 1997). During the very early evolution, the GRB ejecta play a role, and we treat the hydrodynamics of that phase in § 3. The later blast wave, which is dominated by the energy deposited in the external medium, can be described by a self-similar solution (Blandford & McKee 1976). The solution for expansion in a constant-density medium has been widely used in GRB studies, and here we discuss some of the basic results for a medium with density $\rho = Ar^{-s}$, where A is a constant. The main problem is to determine the blast-wave characteristics seen by an external observer.

For an ultrarelativistic, adiabatic blast wave, Blandford & McKee (1976, their eq. [69]) find that

$$E = \frac{8\pi A\Gamma^2 R^{3-s}c^2}{17-4s}, \tag{1}$$

where E is the total energy, Γ is the Lorentz factor of the shock front, and R is the shock-wave radius. The ultrarelativistic shock condition yields the Lorentz factor of the gas, $\gamma = \Gamma/\sqrt{2}$. Because E is constant, we have the standard result $\gamma \propto R^{-(3-s)/2}$. For an observer viewing the blast wave along the line of sight to the center (not at a cosmological distance), consideration of emission from the blast wave at two times in the blast-wave frame yields the time in the observer's frame (e.g., Sari 1997; Panaitescu & Mészáros 1998; Dai & Lu 1998):

$$t = \frac{R_L}{4(4-s)\gamma_L^2 c}, \tag{2}$$

where the subscript L refers to the line of sight. For $s = 0$, we have $t = R_L/(16\gamma_L^2 c)$, as in Sari (1997). For the wind case considered here ($s = 2$), we have $t = R_L/(8\gamma_L^2 c)$ (Dai & Lu 1998). The blast wave is undecelerated for $s = 3$, and we obtain $t = R_L/(4\gamma_L^2 c)$; this can also be expressed as $t = R_L/(2\Gamma_L^2 c)$, which is the standard result for a point moving toward the observer at constant velocity. Substitution into equation (1) then yields

$$R_L = \left[\frac{(4-s)(17-4s)Et}{4\pi Ac}\right]^{1/(4-s)}. \tag{3}$$

We then have $R_L = (17Et/\pi\rho_0 c)^{1/4}$, where ρ_0 is the ambient density, for $s = 0$ and $R_L = (9Et/2\pi Ac)^{1/2}$ for $s = 2$.

The problem with these expressions is that they apply only to the line of sight to the center. In observing a burst, the emission can be dominated by emission away from the center because the burst is observed at an earlier time when it may have been brighter (Waxman 1997c; Panaitescu & Mészáros 1998; Sari 1998). The appearance depends on the evolution of the burst, which itself depends on the observing frequency. Panaitescu & Mészáros (1998) considered these issues for wind and constant-density surroundings and for radiative and nonradiative blast waves. The radius and Lorentz factor of the typical material that is observed can be written as $R = \zeta R_L$ and $\gamma = \zeta^{-1/2}\gamma_L$, where ζ is a constant and the relation between R and γ follows the $\gamma \propto R^{-1/2}$ relation expected for an adiabatic blast wave in a wind. Panaitescu & Mészáros (1998) find $\zeta = 0.56$ at high frequencies where $F_\nu \propto \nu^{-(p-1)/2}$ and $\zeta = 0.78$ at low frequencies where $F_\nu \propto \nu^{1/3}$. We thus have for a distant observer

$$R = 1.1\times 10^{17}\left(\frac{1+z}{2}\right)^{-1/2} E_{52}^{1/2} A_*^{-1/2} t_{\rm days}^{1/2}\ {\rm cm} \tag{4}$$

and

$$\gamma = 5.9\left(\frac{1+z}{2}\right)^{1/4} E_{52}^{1/4} A_*^{-1/4} t_{\rm days}^{-1/4} \tag{5}$$

at high frequencies, where E_{52} is the blast-wave energy in units of 10^{52} ergs, $t_{\rm days}$ is the observer's time in units of days, $A = \dot{M}_w/4\pi V_w = 5\times 10^{11} A_*$ g cm^{-1}, $\dot{M}_w$ is the mass-loss rate, and V_w is the wind velocity. The reference value of A corresponds to $\dot{M}_w = 1\times 10^{-5}\ M_\odot$ yr^{-1} and $V_w = 1000$ km s^{-1} (see CL for a justification of these values in terms of the wind from a Wolf-Rayet star). In addition, the cosmological redshift z enters because of time dilation. At low frequencies, the coefficient in equation (4) is increased to 1.6×10^{17} cm and that in equation (5) is reduced to 5.0.

At early times, the adiabatic assumption is expected to break down because all of the electron energy can be radiated by synchrotron radiation close to the shock front. The importance for the hydrodynamics is determined by the fraction of the total shock energy that goes into the electrons, ϵ_e. The blast wave is radiative either if ϵ_e is close to 1 or if ϵ_e is small, but the magnetic and nucleon energies efficiently couple to the electron energy. In the limiting case, all of the shock power is radiated and we have a radiative blast wave (Blandford & McKee 1976; Vietri 1997; Sari et al. 1998). For $s = 2$, the blast-wave radius along the line of sight is (Böttcher & Dermer 2000)

$$R_{{\rm rad},L} = \left(\frac{3E_0^2 t}{16\pi^2 A^2 c^3 \Gamma_0^2}\right)^{1/3}, \tag{6}$$

where E_0 is the initial energy and Γ_0 is the initial Lorentz factor of the shock front. The evolution of the shock-wave

Lorentz factor is given by

$$\Gamma_{\rm rad,L} = \left(\frac{E_0}{12\pi A^2 c^3 \Gamma_0}\right)^{1/3} t^{-1/3} . \quad (7)$$

The estimated values of ζ for this case are 0.83 (low frequency) and 0.68 (high frequency) (Panaitescu & Mészáros 1998), where now $R = \zeta R_{\rm rad,L}$ and $\Gamma = \zeta^{-1}\Gamma_{\rm rad,L}$.

The limiting radiative case is unlikely to be achieved, and the actual case is probably intermediate between the adiabatic and strongly radiative cases. If $\epsilon = \epsilon_e \epsilon_{\rm rad}$ is a constant, where the synchrotron radiative efficiency $\epsilon_{\rm rad}$ is between 0 and 1, we have (Böttcher & Dermer 2000)

$$R \propto t^{(2-\epsilon)/(4-\epsilon)}, \qquad \gamma \propto t^{-1/(4-\epsilon)} . \quad (8)$$

During the radiative phase, $\epsilon_{\rm rad} \approx 1$, so these expressions apply to the case im which ϵ_e is constant.

2.2. *Afterglow Properties with Slow Cooling*

Our treatment of afterglow light curves in winds follows the discussions of afterglows in a constant-density interstellar medium (Mészáros & Rees 1997; Waxman 1997a, 1997b; Sari et al. 1998; Wijers & Galama 1999). We presume that electrons are accelerated in the blast-wave shock wave to a power energy distribution, $N(\gamma) \propto \gamma^{-p}$ for $\gamma > \gamma_m$, where γ_m is the minimum Lorentz factor at the shock front. The value of γ_m is

$$\gamma_m = \left(\frac{2}{1+X}\right)\left(\frac{m_p}{m_e}\right)\left(\frac{p-2}{p-1}\right)\epsilon_e \gamma , \quad (9)$$

where X is the hydrogen mass fraction, m_p and m_e are the proton and electron masses, respectively, and ϵ_e is again the ratio of the energy density in electrons to the total postshock energy density. Our expression agrees with that of Sari et al. (1998) but differs slightly from that of Wijers & Galama (1999) who identify ϵ_e as the ratio of the energy density in electrons to the postshock *nucleon* energy density. We take $X = 0$ because we are assuming the wind is from a Wolf-Rayet star. The electron energy for which synchrotron losses are important is estimated as that at which the cooling time for electrons with pitch angle $\pi/2$ equals the expansion time:

$$\gamma_c = \frac{6\pi m_e c}{\sigma_{\rm T} \gamma B_{\rm tot}^2 t_{\rm loc}} , \quad (10)$$

where $\sigma_{\rm T}$ is the Thomson cross section, $B_{\rm tot}$ is the total field strength, and $t_{\rm loc} = t/(1+z)$ is the time observed by an observer cosmologically local to the burst.

The synchrotron spectrum of the afterglow can be divided into four power-law sections that are separated at three characteristic frequencies: the synchrotron self-absorption frequency ν_A, the characteristic frequency ν_m emitted by electrons with Lorentz factor γ_m, and the frequency at which synchrotron losses become important ν_c (Sari et al. 1998). If the frequencies are ordered $\nu_A < \nu_m < \nu_c$, the four sections of the spectrum can be described by $F_\nu \propto \nu^\beta$ with (from low to high frequencies) $\beta = 2, \frac{1}{3}, -(p-1)/2, -p/2$. The observations of GRB 970508 on day 12 can be approximately represented by this spectrum (Galama et al. 1998a), and we initially assume this order of the characteristic frequencies in this section. The slow cooling condition can be expressed as $\nu_m < \nu_c$ (Sari et al. 1998). The peak flux, $F_{\nu,\rm max}$, occurs at ν_m for this case.

In any power-law segment of the spectrum, the flux evolution is expected to follow a power law $F_\nu \propto \nu^\beta t^\alpha$. For a constant-density medium ($s = 0$), the standard result is $\alpha = -3(p-1)/4 = 3\beta/2$ for $\nu_m < \nu < \nu_c$ and $\alpha = -(3p-2)/4 = (3\beta+1)/2$ for $\nu_c < \nu$. In a wind ($s = 2$), we have $\alpha = -(3p-1)/4 = (3\beta-1)/2$ for $\nu_m < \nu < \nu_c$ and the same evolution as the $s = 0$ case for $\nu_c < \nu$. A signature of wind interaction afterglows in the noncooling, high-frequency phase of evolution is a relatively rapid rate of decline. The plausible assumption that most of the electron energy is near γ_m requires $p > 2$ and $\alpha < -1.25$. Many optical afterglows are observed to initially have $\alpha \gtrsim -1.3$ and so are unlikely to be in the noncooling, wind category. However, if the optical emission is in the cooling regime, $\alpha = -(3p-2)/4$ as in the $s = 0$ case and the requirement $p > 2$ implies $\alpha < -1.0$. More candidate afterglows are potentially in this category, but there is the additional requirement of a moderately steep observed spectral index: $\beta = -p/2$, so that $p > 2$ implies $\beta < -1.0$.

The observed values of $F_{\nu,\rm max}$, ν_m, ν_A, and ν_c have been used to find the blast-wave energy E, ambient density n, electron energy fraction ϵ_e, and magnetic energy fraction ϵ_B in the context of $s = 0$ models (Wijers & Galama 1999; Granot, Piran, & Sari 1999). In wind models, the constant density is replaced by the wind density $\rho = Ar^{-2}$, where $A = \dot{M}_w/4\pi V_w = 5 \times 10^{11} A_*$ g cm^{-1}, as discussed below equation (5). In CL, expressions were derived for the characteristic frequencies and $F_{\nu,\rm max}$ in terms of the model parameters. We repeat the expressions for completeness:

$$F_{\nu,\rm max} = 20\left(\frac{\sqrt{1+z}-1}{\sqrt{2}-1}\right)^{-2}\left(\frac{1+z}{2}\right)^{1/2} \times \left(\frac{\epsilon_B}{0.1}\right)^{1/2} E_{52}^{1/2} A_* t_{\rm days}^{-1/2} \ {\rm mJy} , \quad (11)$$

$$\nu_A \approx 1 \times 10^{11}\left(\frac{1+z}{2}\right)^{-2/5}\left(\frac{\epsilon_e}{0.1}\right)^{-1} \times \left(\frac{\epsilon_B}{0.1}\right)^{1/5} E_{52}^{-2/5} A_*^{6/5} t_{\rm days}^{-3/5} \ {\rm Hz} , \quad (12)$$

$$\nu_m = 5 \times 10^{12}\left(\frac{1+z}{2}\right)^{1/2}\left(\frac{\epsilon_e}{0.1}\right)^{2}\left(\frac{\epsilon_B}{0.1}\right)^{1/2} E_{52}^{1/2} t_{\rm days}^{-3/2} \ {\rm Hz} , \quad (13)$$

$$\nu_c \approx 2 \times 10^{12}\left(\frac{1+z}{2}\right)^{-3/2}\left(\frac{\epsilon_B}{0.1}\right)^{-3/2} E_{52}^{1/2} A_*^{-2} t_{\rm days}^{1/2} \ {\rm Hz} , \quad (14)$$

where our expressions assume a flat universe with Hubble constant $H_0 = 65$ km s^{-1} Mpc^{-1}. We also assume that the composition of the wind gas is hydrogen depleted and that the electron spectral index is $p \approx 2.5$; the variation due to different values of p is less than other uncertainties. Our expression for ν_c uses the estimate of Sari et al. (1998). The value of ν_c is sensitive to the value of ζ discussed in § 2.1 ($\propto \zeta^5$); we have taken the high-frequency value. The expression for the flux here and elsewhere in the paper can be generalized to any cosmology by replacing $[(1+z)^{1/2} - 1]$ with $d_L/[9.23 \ {\rm Gpc} \ (1+z)^{1/2}]$, where d_L is the luminosity

distance. In the case of a flat universe,

$$d_L = \frac{2c}{H_0}\,(1 + z - \sqrt{1+z})\,. \tag{15}$$

We now invert these expressions in order to solve for the model parameters. The observations are taken to all refer to the same day, t. Then

$$E \approx 3 \times 10^{52} y^3 x^{-1/2} \left(\frac{t}{\text{days}}\right)^{-1/2} \left(\frac{F_{\nu,\max}}{\text{mJy}}\right)^{3/2} \left(\frac{\nu_A}{10^9\ \text{Hz}}\right)^{-5/6} \times \left(\frac{\nu_m}{10^{12}\ \text{Hz}}\right)^{-5/12} \left(\frac{\nu_c}{10^{14}\ \text{Hz}}\right)^{1/4} \text{ergs}\,, \tag{16}$$

$$A_* \approx 9 \times 10^{-4} x \left(\frac{t}{\text{days}}\right)^{2} \left(\frac{\nu_A}{10^9\ \text{Hz}}\right)^{5/3} \times \left(\frac{\nu_m}{10^{12}\ \text{Hz}}\right)^{5/6} \left(\frac{\nu_c}{10^{14}\ \text{Hz}}\right)^{1/2}, \tag{17}$$

$$\epsilon_e \approx 0.006\, y^{-1} x^{1/2} \left(\frac{t}{\text{days}}\right)^{3/2} \left(\frac{F_{\nu,\max}}{\text{mJy}}\right)^{-1/2} \left(\frac{\nu_A}{10^9\ \text{Hz}}\right)^{5/6} \times \left(\frac{\nu_m}{10^{12}\ \text{Hz}}\right)^{11/12} \left(\frac{\nu_c}{10^{14}\ \text{Hz}}\right)^{1/4}, \tag{18}$$

$$\epsilon_B \approx 1 \times 10^{2} y x^{-5/2} \left(\frac{t}{\text{days}}\right)^{-5/2} \left(\frac{F_{\nu,\max}}{\text{mJy}}\right)^{-1/2} \left(\frac{\nu_A}{10^9\ \text{Hz}}\right)^{-5/2} \times \left(\frac{\nu_m}{10^{12}\ \text{Hz}}\right)^{-5/4} \left(\frac{\nu_c}{10^{14}\ \text{Hz}}\right)^{-5/4}, \tag{19}$$

where

$$x = \frac{1+z}{2} \quad \text{and} \quad y = \frac{\sqrt{2x} - 1}{\sqrt{2} - 1}\,.$$

The afterglow light curve depends on how the break frequencies and the peak flux, $F_{\nu,\max}$, evolve with time and here we consider the light curve without cooling. As in Sari et al. (1998) for the ISM case, we can define critical times at which the break frequencies pass through a fixed frequency ν. The time that ν_m crosses the observed frequency is

$$t_m = 60 \left(\frac{1+z}{2}\right)^{1/3} \left(\frac{\epsilon_e}{0.1}\right)^{4/3} \left(\frac{\epsilon_B}{0.1}\right)^{1/3} E_{52}^{1/3}\, \nu_{10}^{-2/3}\ \text{days}\,, \tag{20}$$

where ν_{10} is ν in units of 10^{10} Hz. The time that ν_A crosses the observed frequency is

$$t_A = 50 \left(\frac{1+z}{2}\right)^{-2/3} \left(\frac{\epsilon_e}{0.1}\right)^{5/3} \left(\frac{\epsilon_B}{0.1}\right)^{1/3} E_{52}^{-2/3}\, A_*^2\, \nu_{10}^{-5/3}\ \text{days}\,. \tag{21}$$

Provided $t_A < t_m$, the light curve is as follows: $F_\nu \propto R^2 \propto t$ for $t < t_A$, $F_\nu \propto F_{\nu,\max} \nu_m^{-1/3} \propto t^0$ for $t_A < t < t_m$, and $F_\nu \propto F_{\nu,\max} \nu_m^{(p-1)/2} \propto t^{-(3p-1)/4}$ for $t_m < t$. The condition that $t_A = t_m$ leads to a critical time and frequency:

$$t_{Am} = 80 \left(\frac{1+z}{2}\right) \left(\frac{\epsilon_e}{0.1}\right)^{10/3} \left(\frac{\epsilon_B}{0.1}\right)^{1/3} E_{52}\, A_*^{-4/3}\ \text{days} \tag{22}$$

and

$$\nu_{Am} = 7 \times 10^{9} \left(\frac{1+z}{2}\right)^{-1} \left(\frac{\epsilon_e}{0.1}\right)^{-3} E_{52}^{-1}\, A_*^2\ \text{Hz}\,. \tag{23}$$

For $\nu > \nu_{Am}$, the light curve is as described above.

For $\nu < \nu_{Am}$, there is a regime where the spectrum is characterized by $\nu_m < \nu_A$. In general, the flux in the self-absorbed part of the spectrum can be described by $F_\nu \propto R^2 \nu^2 (\gamma_e/\gamma_m)$, where γ_e is the Lorentz factor of the electrons that are responsible for the emission at frequency ν. Then, for $\nu < \nu_m$, $\gamma_e = \gamma_m$ and $F_\nu \propto t\nu^2$ as before. For $\nu_m < \nu < \nu_A$, $(\gamma_e/\gamma_m) = (\nu/\nu_m)^{1/2}$ so that $F_\nu \propto t^{7/4} \nu^{5/2}$. Above ν_A, we again have $F_\nu \propto t^{-(3p-1)/4} \nu^{-(p-1)/2}$; the $\nu^{1/3}$ part of the spectrum is no longer present. The evolution of ν_m is always $\propto t^{-3/2}$, but now $F_{\nu_m} \propto t^{-2}$. The peak of the spectrum is at $\nu_A \propto t^{-[3(2+p)]/[2(4+p)]}$, and $F_{\nu_A} \propto t^{-(1+4p)/[2(4+p)]}$. The light curve is thus described by $F_\nu \propto t\nu^2$ up to $t = t_m$, followed by $F_\nu \propto t^{7/4} \nu^{5/2}$ and $F_\nu \propto t^{-(3p-1)/4} \nu^{-(p-1)/2}$. It can be seen from the estimated value of ν_{Am} that these considerations are relevant to radio observations of afterglows.

2.3. *Fast Cooling Case*

The description of the evolution given in CL and in §2.2 assumes that $\nu_m < \nu_c$. Although synchrotron cooling is important for the high-energy electrons, it is not important for the electrons emitting near ν_m which have most of the energy. Before some time, t_0, when $\nu_m = \nu_c$, cooling of these lower energy electrons is rapid compared to the age and this phase can be referred to as having fast cooling (Sari et al. 1998). If ϵ_e is close to 1, the blast wave steadily loses energy and the hydrodynamic evolution is termed radiative. If ϵ_e is small, the hydrodynamic evolution is approximately adiabatic even for $t < t_0$. We consider this second case to be the most likely and concentrate on it. For $\nu_m > \nu_c$, the expressions for $F_{\nu,\max}$, ν_m, and ν_c (eqs. [11], [13], and [14]) remain unchanged; the maximum flux now occurs at ν_c instead of ν_m. The spectrum can be described by $F_\nu \propto \nu^\beta$ with (from low to high frequencies) $\beta = \frac{1}{3}, -\frac{1}{2}, -p/2$ and the breaks at ν_c and ν_m, respectively (Sari et al. 1998). However, equation (12) for ν_A is no longer applicable.

Equations (13) and (14) imply that

$$t_0 = 2 \left(\frac{1+z}{2}\right) \left(\frac{\epsilon_e}{0.1}\right) \left(\frac{\epsilon_B}{0.1}\right) A_*\ \text{days}\,. \tag{24}$$

For standard parameters, the transition to slow cooling occurs at a later time for the wind case compared to the ISM case because of the higher densities that the shock front encounters at early times.

The afterglow light curve again depends on how the break frequencies and the peak flux, $F_{\nu,\max}$, evolve with time. The cooling time for the wind case is

$$t_c = 2 \times 10^{-5} \left(\frac{1+z}{2}\right)^{3} \left(\frac{\epsilon_B}{0.1}\right)^{3} E_{52}^{-1}\, A_*^4\, \nu_{10}^2\ \text{days}\,. \tag{25}$$

The effects of cooling at a frequency ν are important for $t < t_c$, and fast cooling can affect the blast-wave evolution up to time t_0, so cooling has effects up to $t = \max(t_c, t_0)$. The time that ν_m crosses ν is given by equation (20). There are two possible orders for the three times: $t_m < t_0 < t_c$ and $t_c < t_0 < t_m$. These cases are divided by a critical frequency, $\nu_0 = \nu_c(t_0) = \nu_m(t_0)$:

$$\nu_0 = 3 \times 10^{12} \left(\frac{1+z}{2}\right)^{-1} \left(\frac{\epsilon_e}{0.1}\right)^{1/2} \left(\frac{\epsilon_B}{0.1}\right)^{-1} E_{52}^{1/2}\, A_*^{-3/2}\ \text{Hz}\,. \tag{26}$$

When $\nu > \nu_0$, the order $t_m < t_0 < t_c$ applies and the evolution can be called the high-frequency light curve (cf. Sari et al. 1998 for the ISM case). The evolution is described by $F_\nu \propto t^{-1/4}\nu^{-1/2}$ $(t < t_m)$, $t^{-(3p-2)/4}\nu^{-p/2}$ $(t_m < t < t_0)$, $t^{-(3p-2)/4}\nu^{-p/2}$ $(t_0 < t < t_c)$, and $t^{-(3p-1)/4}\nu^{-(p-1)/2}$ $(t_c < t)$. When $\nu < \nu_0$, $t_c < t_0 < t_m$ applies and we have the low-frequency light curve: $F_\nu \propto t^{-1/4}\nu^{-1/2}$ $(t < t_c)$, $t^{-2/3}\nu^{1/3}$ $(t_c < t < t_0)$, $t^0\nu^{1/3}$ $(t_0 < t < t_m)$, and $t^{-(3p-1)/4}\nu^{-(p-1)/2}$ $(t_m < t)$. These light curves are distinct from the ISM case, especially because of the early importance of cooling.

Self-absorption is important throughout the cooling regime $(t < t_0)$ if $t_A > t_0$. From equations (22) (which assumes the low-frequency light curve) and (24), the frequency at which $t_A = t_0$ is given by

$$\nu_{Ao} = 8 \times 10^{10}\left(\frac{1+z}{2}\right)^{-1}\left(\frac{\epsilon_e}{0.1}\right)^{-8/5} \times \left(\frac{\epsilon_B}{0.1}\right)^{-2/5} E_{52}^{-2/5} A_*^{3/5} \text{ Hz} . \quad (27)$$

With typical parameters, $\nu_{Ao} < \nu_0$, so the use of equation (22) is justified. At radio wavelengths, the synchrotron emission is self-absorbed during the fast cooling period. At optical and X-ray wavelengths, self-absorption is important only during the early phases of the fast cooling period.

The effects of self-absorption during the fast cooling period can be found in the same way as described above. The frequencies ν_m and ν_c are again given by the standard expressions (eqs. [13] and [14]), and the behavior of ν_A can be found by considering the complete spectral evolution. For the cases $\nu_A < \nu_c < \nu_m$ and $\nu_c < \nu_A < \nu_m$, the high-frequency properties are the same. For $\nu > \nu_m$, $F_\nu \propto t^{-(3p-2)/4}\nu^{-p/2}$ and for ν below ν_m, we have $F_\nu \propto t^{-1/4}\nu^{-1/2}$. We also have $F_{\nu_m} \propto t^{1/2}$. In the lowest frequency range, where self-absorption is important, the electrons responsible for the emission have a Lorentz factor corresponding to peak emission at ν_c. The evolution is thus given by $F_\nu \propto R^2(\nu_c/\nu_m)^{1/2} \propto t^2\nu^2$. For $\nu_A < \nu_c$, it is now straightforward to show that $\nu_A \propto t^{-8/5}$, $F_{\nu_A} \propto t^{-6/5}$, $F_{\nu_c} \propto t^{-1/2}$, and $F_\nu \propto t^{-2/3}\nu^{1/3}$ for $\nu_A < \nu < \nu_c$. For $\nu_c < \nu_A$, we have $\nu_A \propto t^{-2/3}$, $F_{\nu_c} \propto t^3$, $F_{\nu_a} \propto t^{1/12}$, and $F_\nu \propto t^{7/4}\nu^{5/2}$ for $\nu_c < \nu < \nu_A$.

2.4. *Light Curves*

The consideration of complete light curves for relativistic, spherical expansion involves the combination of both cooling and adiabatic evolution. At a particular frequency, cooling effects are important up to a time $t = \max(t_0, t_c)$. The relevant transition times for a light curve are t_A, t_0, t_c, and t_m. These four transition times allow many possible light curves, but our previous discussion allows us to limit the possibilities, on the assumption that the blast-wave conditions are not far from the typical conditions that we have chosen. In particular, equations (22) and (23) show that we expect $t_A = t_m$ at a relatively late time and low frequency. We thus expect $t_A < t_m$ at higher frequencies, including all those in the high-frequency case with regard to radiative cooling.

The orders of the transition times of interest are thus (A) $t_A < t_m < t_0 < t_c$; (B) $t_A < t_c < t_0 < t_m$; (C) $t_c < t_A < t_0 < t_m$; (D) $t_c < t_0 < t_A < t_m$; and (E) $t_c < t_0 < t_m < t_A$, where the listing is from high-frequency to low-frequency light curves. The frequency dividing light curve A from B is ν_0 (eq. [26]), that dividing C from D is ν_{Ao} (eq. [27]), and that dividing D from E is ν_{Am} (eq. [23]). The frequency dividing curve B from C is that at which $t_c = t_A$. By referring to the previous sections, the light curves for each case can be constructed. They are (A) $F_\nu \propto t^{7/4}\nu^{5/2}$ $(t < t_A)$, $t^{-1/4}\nu^{-1/2}$ (t_A, t_m), $t^{-(3p-2)/4}\nu^{-p/2}$ (t_m, t_0), $t^{-(3p-2)/4}\nu^{-p/2}$ (t_0, t_c), $t^{-(3p-1)/4}\nu^{-(p-1)/2}$ $(t_c < t)$; (B) $F_\nu \propto t^{7/4}\nu^{5/2}$ $(t < t_A)$, $t^{-1/4}\nu^{-1/2}$ (t_A, t_c), $t^{-2/3}\nu^{1/3}$ (t_c, t_0), $t^0\nu^{1/3}$ (t_0, t_m), $t^{-(3p-1)/4}\nu^{-(p-1)/2}$ $(t_m < t)$; (C) $F_\nu \propto t^{7/4}\nu^{5/2}$ $(t < t_c)$, $t^2\nu^2$ (t_c, t_A), $t^{-2/3}\nu^{1/3}$ (t_A, t_0), $t^0\nu^{1/3}$ (t_0, t_m), $t^{-(3p-1)/4}\nu^{-(p-1)/2}$ $(t_m < t)$; (D) $F_\nu \propto t^{7/4}\nu^{5/2}$ $(t < t_c)$, $t^2\nu^2$ (t_c, t_0), $t\nu^2$ (t_0, t_A), $t^0\nu^{1/3}$ (t_A, t_m), $t^{-(3p-1)/4}\nu^{-(p-1)/2}$ $(t_m < t)$; (E) $F_\nu \propto t^{7/4}\nu^{5/2}$ $(t < t_c)$, $t^2\nu^2$ (t_c, t_0), $t\nu^2$ (t_0, t_m), $t^{7/4}\nu^{5/2}$ (t_m, t_A), $t^{-(3p-1)/4}\nu^{-(p-1)/2}$ $(t_A < t)$. The times in parentheses give the time range for that particular section of the light curve. The light curves are illustrated in Figure 1. In the figure, t_A is omitted from curve A and t_c from curves D and E because they occur at very early times.

For our typical parameters, both X-ray and optical light curves are of type A. It can be seen from equation (20) that t_m is typically in the tens of seconds range at these high frequencies. The self-absorbed part of the light curve occurs considerably earlier, when the shock evolution is still affected by the energy deposition and our model is not applicable. The radio light curve is typically of type D. The light curve properties are like those described by CL, except we have now found that a steeper rise is expected for $t < t_0$.

For the above light curves, we have assumed that the hydrodynamic evolution is described by an adiabatic blast wave. For $t < t_0$, the energy loss by electrons can affect the evolution. In § 2.1, we gave the expected evolution for a fully radiative blast wave. In this case for a $\rho \propto r^{-2}$ ambient medium, standard expressions (Sari et al. 1998; Wijers & Galama 1999) yield $\nu_c \propto t^{1/3}$, $\nu_m \propto t^{-5/3}$, and $F_{\nu,\max} \propto t^{-2/3}$. We thus have $F_\nu = F_{\nu,\max}(\nu/\nu_c)^{1/3} \propto t^{-7/9}\nu^{1/3}$ for $\nu_A < \nu < \nu_c$, $F_\nu = F_{\nu,\max}(\nu/\nu_c)^{-1/2} \propto t^{-1/2}\nu^{-1/2}$ for $\nu_c < \nu < \nu_m$, and $F_\nu = F_{\nu_m}(\nu/\nu_m)^{-p/2} \propto t^{-(5p-2)/6}\nu^{-p/2}$ for $\nu_m < \nu$. The evolution at optical and X-ray wavelengths is most likely to be in the $\nu_m < \nu$ regime; for $p = (2.0,2.5,3.0)$, the evolution of a radiative blast wave is given by $F_\nu \propto t^{(-1.33,-1.75,-2.17)}$, as compared to $F_\nu \propto t^{(-1.00,-1.38,-1.75)}$ for an adiabatic blast wave. There is a significant steepening of the light curve for the radiative case. The radio light curve is likely to be in the self-absorbed regime. For $\nu < \nu_A, \nu_c$, we have $F_\nu \propto R^2\nu^2(\nu_c/\nu_m)^{1/2} \propto t^{5/3}\nu^2$.

The actual situation is likely to be intermediate between adiabatic and radiative evolution of the blast wave, and we use equation (8) to find the time dependences in that case. We find $\nu_c \propto t^{(2-\epsilon)/(4-\epsilon)}$, $\nu_m \propto t^{-(6-\epsilon)/(4-\epsilon)}$, and $F_{\nu,\max} \propto t^{-2/(4-\epsilon)}$. The resulting flux evolution for $\nu > \nu_m$ is $F_\nu \propto t^{-[(6-\epsilon)p-2(2-\epsilon)]/[2(4-\epsilon)]}\nu^{-p/2}$. Thus, for $\epsilon = 0.1$, we have $F_\nu \propto t^{(-1.03,-1.40,-1.78)}$ for $p = (2.0,2.5,3.0)$, and for $\epsilon = \frac{1}{3}$ we have $F_\nu \propto t^{(-1.09,-1.48,-1.86)}$. It can be can that the change from the adiabatic case is small for $\epsilon = 0.1$ but becomes significant for $\epsilon = \frac{1}{3}$. The radio evolution is likely to be characterized by $\nu < \nu_A$, which is below ν_c and ν_m. We then have $F_\nu \propto t^{(8-3\epsilon)/(4-\epsilon)}\nu^2$.

2.5. *Transition to Nonrelativistic Evolution*

The transition to nonrelativistic evolution has been discussed for the ISM, constant-density case by Wijers et al. (1997) and Waxman, Kulkarni, & Frail (1998). For an ambient density $\rho = Ar^{-2}$, a straightforward estimate of the transition radius and time is when the shock has swept up a

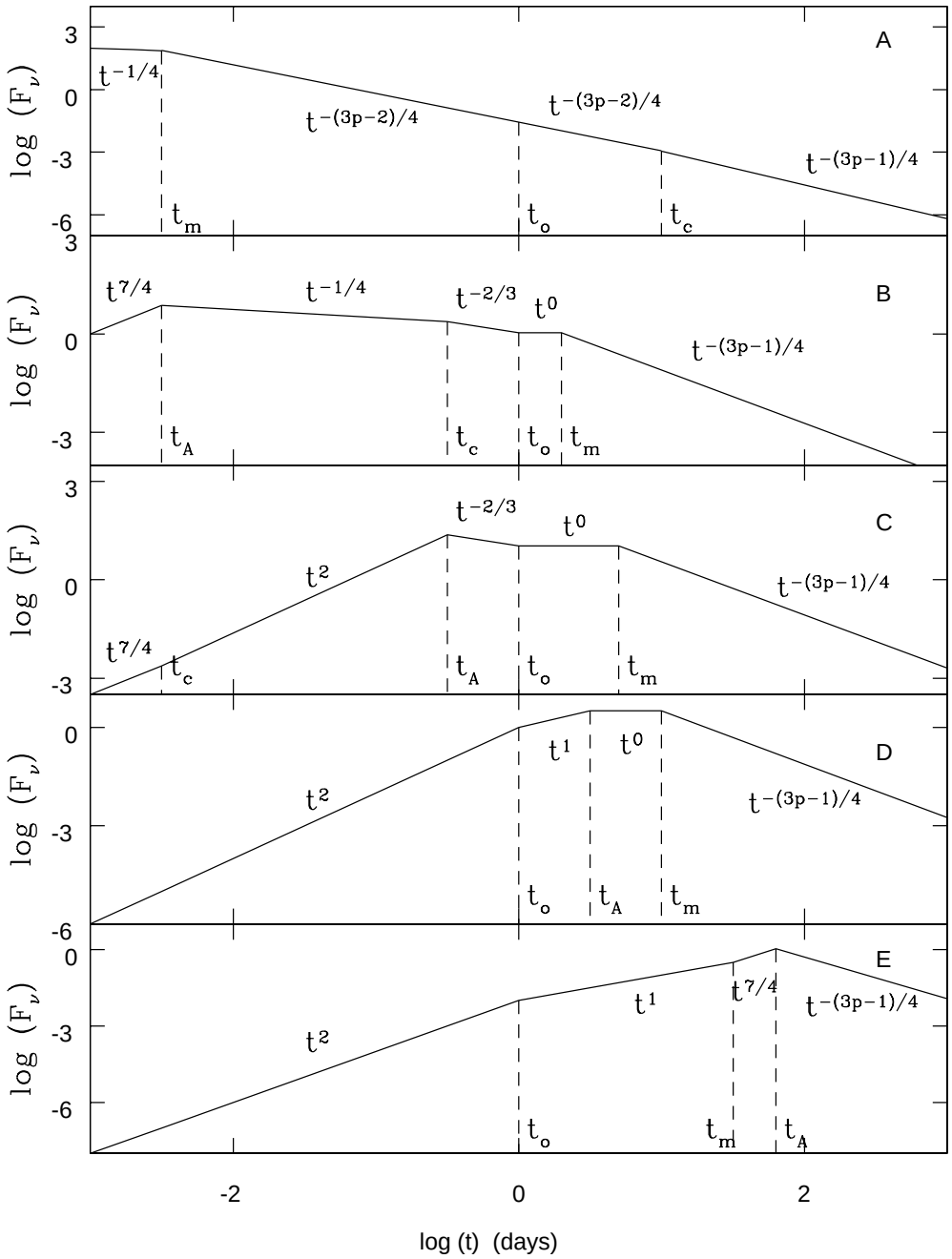

FIG. 1.—Characteristic light curves for wind interaction models in various frequency ranges. The light curves are sorted from (*a*) high frequency (type A) to (*e*) low frequency (type E). X-ray and optical light curves are typically of type A and radio of type D.

mass equivalent to the rest mass of the explosion:

$$r_{\rm NR} = \frac{E}{4\pi A c^2} = 1.8 \times 10^{18} \frac{E_{52}}{A_*} \text{ cm} \qquad (28)$$

and

$$t_{\rm NR} = \frac{r_{\rm NR}}{c} = 1.9(1+z) \frac{E_{52}}{A_*} \text{ yr} . \qquad (29)$$

From equation (5), the relativistic blast-wave shock Lorentz factor at this time is $\Gamma = 1.38$ (high-frequency observation) or $\Gamma = 1.17$ (low-frequency observation).

The nonrelativistic blast wave in a $\rho = Ar^{-2}$ medium is particularly simple for adiabatic index $\gamma_a = 5/3$ (e.g., Sedov 1959). The shock radius is given by

$$r_s = \left(\frac{3E}{2\pi A}\right)^{1/3} t^{2/3} , \qquad (30)$$

and the postshock profiles are $\rho = \rho_s(r/r_s)$, $v = v_{gs}(r/r_s)$, and $p = p_s(r/r_s)^3$, where the subscript s refers to the value at the shock front and v_{gs} is the gas velocity at the shock front. The blast-wave expansion can be described by $r_s = \xi_0(E/A)^{1/3}t^{2/3}$, where $\xi_0 = 0.78$ if $\gamma_a = 5/3$ (nonrelativistic fluid) and $\xi_0 = 0.64$ if $\gamma_a = 4/3$ (relativistic fluid). The $\gamma_a = 5/3$ evolution yields $\dot{r}_s/c = 1.2$ at the time $t_{\rm NR}$. The relativistic and nonrelativistic expansion approximately cross at $t_{\rm NR}$, showing that this is a reasonable estimate of the transition time. Equation (29) shows that the transition to

nonrelativistic evolution in a wind is late for typical parameters; the expected value of $t_{\rm NR}$ is longer than the typical duration of observations of GRB afterglows.

In considering the evolution during the nonrelativistic regime, the treatment is similar to that in the relativistic regime provided $\gamma_m \gtrsim 1$. We have $R \propto t^{2/3}$, shock velocity $v_{sh} \propto t^{-1/3}$, $\rho_1 v_{sh}^2 \propto t^{-2}$, $B \propto t^{-1}$, and $\gamma_m \propto v_{sh}^2 \propto t^{-2/3}$, so $\nu_m \propto \gamma_m^2 B \propto t^{-7/3}$ and $F_{\nu_m} \propto NB \propto Rt^{-1} \propto t^{-1/3}$, where ρ_1 is the preshock density and N is the total number of radiating particles. Then, $F_\nu \propto F_{\nu_m} \nu_m^{-1/3} \propto t^{4/9}$ $(\nu < \nu_m)$ and $F_\nu \propto F_{\nu_m} \nu_m^{(p-1)/2} \propto t^{(5-7p)/6}$ $(\nu > \nu_m)$. For example, $p = 3$ yields $F_\nu \propto t^{-8/3}$ in the nonrelativistic case for $\nu > \nu_m$ but $F_\nu \propto t^{-2}$ in the relativistic case. As in interstellar interaction, the light curve steepens after the transition to nonrelativistic flow.

2.6. *Jets*

In most models for GRBs, the burst energy is initially deposited in a relativistic jet. As long as the jet is highly relativistic, the observed features should be reproduced by spherical models, but as the shocked jet slows there are effects on the observed light curve (as first discussed by Rhoads 1997). If θ_0 is the angular width of the jet, the edge of the jet becomes visible when $\gamma \approx \theta_0^{-1}$ (Panaitescu & Mészáros 1999). The other important effect is that the slowed jet is able to expand laterally. Rhoads (1997, 1999) estimates that this will occur when $\gamma \approx \theta_0^{-1}/\sqrt{3}$, but Sari et al. (1999) argue that the transition occurs when $\gamma \approx \theta_0^{-1}$. The issue is the speed of sideways expansion and two-dimensional numerical simulations may be needed to provide reliable results. The important point is that during the spreading phase, there is exponential slowing down of the forward shock front (Rhoads 1997). Rhoads (1999) has discussed this phenomenon in detail for interstellar interaction but suggests that it also occurs for expansion in a wind.

Because jet effects are expected when $\gamma \approx \theta_0^{-1}$, equation (5) can be used to find the time

$$t_{\rm jet} = 2\left(\frac{1+z}{2}\right)\left(\frac{\theta_0}{0.2}\right)^4 E_{52} A_*^{-1} \text{ days} \tag{31}$$

when jet effects become important. This expression is appropriate for high frequencies; at low frequencies (radio), the coefficient becomes 1 day. A steepening of the afterglow light curve is expected at $t_{\rm jet}$. Once lateral spreading of the jet becomes important, the rapid slowing implies that R becomes essentially constant with time and this defines the hydrodynamic evolution (Sari et al. 1999). The general nature of the slow expansion is shown by the conservation of energy, $E \approx c^2 \rho_1 R^3 \gamma^2 \Omega$, where ρ_1 is the preshock density and Ω is the solid angle of the jet. During the jet spreading phase $\Omega \propto \gamma^{-2}$ (Rhoads 1997, 1999; Sari et al. 1999) and $E \approx c^2 \rho_1 R^3$, so R must be a weaker function of γ than any power law, independent of the density profile.[1] Thus, both ISM and wind interactors should show the same emission properties during the spreading phase. We expect $F_\nu \propto t^0 \nu^2$ $(\nu < \nu_A)$, $t^{-1/3}\nu^{1/3}$ $(\nu_A < \nu < \nu_m)$, $t^{-p}\nu^{-(p-1)/2}$ $(\nu_m < \nu < \nu_c)$, and $t^{-p}\nu^{-p/2}$ $(\nu_c < \nu)$ (Sari et al. 1999).

3. PROMPT, REVERSE-SHOCK EMISSION

An initially relativistically hot fireball associated with a GRB cools as it expands, forming a cold shell of material coasting at an ultrarelativistic speed when most of the internal energy is converted into the bulk kinetic energy. When the coasting shell runs into an ambient medium, the bulk kinetic energy is gradually released back into the internal energy, which gives rise to prompt emission. Prompt emission has been discussed by Sari & Piran (1999a, 1999b) and Mészáros & Rees (1999) in the context of GRB 990123, both assuming a constant ambient density suitable for the interstellar medium. In § 3.1, we extend their discussion of prompt emission to the case of a stellar wind as the ambient medium. A comparison with the ISM case is presented in § 3.2.

3.1. *Wind Interaction Case*

The structure of the coasting shell is largely unknown and is determined by the way that mass and energy are injected from the central engine. It is likely to be inhomogeneous, since bursts of gamma rays are thought to come from one part of the shell running into another. We shall, however, ignore such inhomogeneities and adopt uniform distributions for both the shell density and Lorentz factor (denoted by $\gamma_{\rm sh}$) for simplicity.

As is well known, the shell interacts with the ambient medium via two shocks: a forward shock and a reverse shock. The forward shock runs forward into the ambient medium, whereas the reverse shock sweeps up the shell material. The shocked ambient and shell materials are in pressure balance and are separated by a contact continuity. Since the thickness of the shocked region is expected to be much smaller than its radius, the whole interaction region can be treated as planar, as done by Katz (1994) and Sari & Piran (1995). We will follow these authors in determining the shock properties in a planar geometry, assuming in addition that only a small fraction of the internal energy of the shocked materials is radiated away by electrons.

There are four regions of distinct properties: the unshocked ambient medium (denoted "1"), the shocked ambient medium ("2"), the shocked shell material ("3"), and the unshocked coasting shell ("4"). We assume that the shocked materials in regions 2 and 3 are uniform and move together and thus share a common bulk Lorentz factor. From relativistic shock jump conditions, we find that the Lorentz factor is

$$\gamma_{12} = \frac{\xi^{1/4}\gamma_{\rm sh}^{1/2}}{\sqrt{2}}, \tag{32}$$

(measured relative to the nearly static ambient medium, region 1) where $\xi \equiv \rho_4/\rho_1$ is the ratio of proper mass densities in the unshocked shell (region 4) and the ambient medium (region 1). The proper mass density in the ambient medium is given by

$$\rho_1 = \frac{\dot{M}_w}{4\pi R^2 V_w}, \tag{33}$$

where $\dot{M}_w$ and V_w are the mass-loss rate and the velocity of the ambient wind, and R the spherical radius. The proper density of the unshocked shell is given by

$$\rho_4 = \frac{M_{\rm sh}}{4\pi R^2 \gamma_{\rm sh} \Delta}, \tag{34}$$

where $M_{\rm sh}$ and Δ are the proper mass and the width (measured in the frame at rest with respect to the origin and the ambient medium and cosmologically local to the burst)

[1] Re'em Sari pointed out this argument.

of the initial shell. The proper mass is related to the total initial kinetic energy E_0 of the coasting shell through

$$M_{\rm sh} = \frac{E_0}{\gamma_{\rm sh} c^2}\,, \tag{35}$$

where c is the speed of light. From equations (33)–(35), we have

$$\xi = \frac{E_0 V_w}{\dot{M}_w \gamma_{\rm sh}^2 c^2 \Delta}\,, \tag{36}$$

which is independent of radius. Therefore, the shocked materials move at a constant speed according to equation (32). This fact simplifies our discussion of their emission properties.

The initial shell width Δ is unknown a priori. It is related to the time $T_{\rm cr}$ in the frame at rest with respect to the origin and cosmologically local to the burst for the reverse shock to cross the entire shell through

$$T_{\rm cr} = \frac{\gamma_{12}^2 \Delta}{c}\,. \tag{37}$$

The radiation emitted at this time by the shocked shell material along the line of sight is received by an observer on Earth at different times, ranging from $(1 + z)\Delta/(2c)$ (for radiation emitted near the contact discontinuity) to $(1 + z)\Delta/c$ (for radiation emitted immediately behind the reverse shock). The timescale, Δ/c, therefore characterizes the duration of prompt emission (see Sari & Piran 1999b). We assume that the duration is comparable to that of the GRB itself, which is typically tens of seconds for the sources with observed afterglows. That is, the shell needs to have a width of tens of light seconds or more. We shall therefore scale Δ by 10 light seconds and denote the scaled width by Δ_{10}. Scaling other quantities with their typical values, we have

$$\xi = 5.9\,\frac{E_{52}}{A_* \Delta_{10} \gamma_3^2}\,, \tag{38}$$

where γ_3 is the unshocked shell Lorentz factor $\gamma_{\rm sh}$ divided by 10^3 (not to be mistaken as the Lorentz factor of region 3). In deriving equation (37), we have assumed that $\xi \ll \gamma_{\rm sh}^2$, which is true for typical parameters. Substituting equation (38) into equation (32), we finally have

$$\gamma_{12} = 35\,\frac{E_{52}^{1/4}}{A_*^{1/4} \Delta_{10}^{1/4}}\,, \tag{39}$$

which is much greater than unity unless Δ_{10}, the most uncertain parameter in the above expression, is unreasonably large.

The shocked ambient medium and the shocked shell material have not only the same bulk Lorentz factor but also the same internal energy density because of pressure balance across the contact discontinuity. Relativistic shock jump conditions yield

$$e_3 = e_2 = 2\gamma_{\rm sh} \rho_1 c^2 \xi^{1/2}\,, \tag{40}$$

where the mass density of the ambient wind is given by equation (33), which can be rewritten into

$$\rho_1 = \frac{\dot{M}_w}{4\pi V_w R^2} = \frac{\dot{M}_w}{4\pi V_w c^2 T^2}\,, \tag{41}$$

with the time T measured in the frame at rest with respect to the origin and cosmologically local to the burst. As usual, we assume a (small) fraction ϵ_e of the internal energy of the shocked matter goes into radiating electrons with a power-law energy distribution. Adopting a constant power-law index of p, the minimum electron Lorentz factors in the two shocked regions are

$$\gamma_{m2} = \left(\frac{p-2}{p-1}\right)\left(\frac{2}{1+X}\right)\left(\frac{m_p}{m_e}\right)\frac{\epsilon_{e2}\,\gamma_{\rm sh}^{1/2}\,\xi^{1/4}}{\sqrt{2}} \tag{42}$$

and

$$\gamma_{m3} = \left(\frac{p-2}{p-1}\right)\left(\frac{2}{1+X}\right)\left(\frac{m_p}{m_e}\right)\frac{\epsilon_{e3}\,\gamma_{\rm sh}^{1/2}}{\sqrt{2}\xi^{1/4}}\,, \tag{43}$$

where m_p and m_e are the mass of protons and electrons, respectively, and X is the fractional abundance of hydrogen, which is close to zero for hydrogen depleted Wolf-Rayet winds. In addition, we assume that a constant fraction ϵ_B of the internal energy goes into the magnetic field in both the shocked ambient medium and the shocked shell material, which yields a total field strength of

$$B_{\rm tot} = (8\pi\epsilon_B e_2)^{1/2} = \left(\frac{4\epsilon_B \gamma_{\rm sh} \dot{M}_w \xi^{1/2}}{V_w}\right)^{1/2}\frac{1}{T} \tag{44}$$

in regions 2 and 3.

To determine the shock emission properties, we adopt the formalism of Sari et al. (1998), including cosmological corrections. Let us first consider the reverse shock (region 3). Ignoring the synchrotron self-absorption for the moment, there are two characteristic frequencies that we need to determine: the "typical" frequency ν_{m3} corresponding to the minimum Lorentz factor γ_{m3} and the cooling frequency ν_c. In the observer's frame, we find

$$\begin{aligned}\nu_{m3} &= \left(\frac{1}{1+z}\right)\frac{\gamma_{12}\gamma_{m3}^2 eB_{\rm tot}}{2\pi m_e c} \\ &= 9.8\times 10^{18}\left(\frac{3p-6}{p-1}\right)^2\left(\frac{1}{1+X}\right)^2 \\ &\quad\times\left(\frac{\epsilon_{e3}}{0.1}\right)^2\left(\frac{\epsilon_B}{0.1}\right)^{1/2}\frac{A_*\Delta_{10}^{1/2}\gamma_3^2}{E_{52}^{1/2}\,t}\ {\rm Hz}\,,\end{aligned} \tag{45}$$

where e is the charge of electron and the factor $(3p - 6)/(p - 1)$ equals unity for $p = 2.5$. We have related the observer's time t to the time T in the frame at rest with respect to the origin through[2]

$$t = \frac{1+z}{2}\,\frac{T}{\gamma_{12}^2}\,. \tag{46}$$

The typical frequency ν_{m3} shown in equation (45) is to be compared with the cooling frequency ν_c corresponding to the cooling Lorentz factor given by equation (10) with $\gamma =$

[2] Strictly speaking, the radiation emitted at time T from the shocked material along the line of sight between the forward and reverse shocks arrives at the observer at different times. The observed times are $(1 + z)T/\gamma_{12}^2$, $(1 + z)T/(2\gamma_{12}^2)$, and $(1 + z)T/(4\gamma_{12}^2)$ for the radiation emitted at time T from the reverse-shock front, the contact continuity, and the forward shock front, respectively. We pick $t = (1 + z)T/(2\gamma_{12}^2)$ as a compromise between the reverse shock and the forward shock, since the emission from both regions will be computed.

γ_{12}. The cooling frequency observed on Earth is then

$$\nu_c = \left(\frac{1}{1+z}\right)\frac{\gamma_{12}\gamma_c^2 eB_{\rm tot}}{2\pi m_e c} = 3.6\times 10^8\left(\frac{2}{1+z}\right)^2\left(\frac{\epsilon_B}{0.1}\right)^{-3/2}\frac{E_{52}^{1/2}\,t}{A_*^2\,\Delta_{10}^{1/2}}\ {\rm Hz}\ . \quad (47)$$

Clearly, the cooling frequency is much lower than the typical frequency for reasonable parameters, indicating that most radiating electrons cool quickly down to the cooling Lorentz factor γ_c. In other words, the shocked shell material is in the fast cooling regime of Sari et al. (1998). The emitted flux density therefore peaks at ν_c instead of ν_{m3}, with a peak value given approximately by

$$F_{\nu_c,3} = \frac{N_{e,3}(1+z)P_{\nu,\max}}{4\pi d_L^2}\ , \quad (48)$$

where the number of radiating electrons $N_{e,3}$ in the shocked shell region increases linearly with time as

$$N_{e,3} = \left(\frac{2}{1+z}\right)\left(\frac{1+X}{2}\right)\frac{E_0\,t}{\gamma_{\rm sh}\,m_p\,c\Delta}\ . \quad (49)$$

The peak spectral power $P_{\nu,\max}$ is given roughly by

$$P_{\nu,\max} = \frac{m_e c^2\sigma_{\rm T}\gamma_{12}B_{\rm tot}}{3e}\ . \quad (50)$$

Substituting equations (15), (49), and (50) into equation (48), we arrive at an approximate peak flux at the cooling frequency of

$$F_{\nu_c,3} = 16(1+X)\left(\frac{1+z}{2}\right)\times\left(\frac{2-\sqrt{2}}{1+z-\sqrt{1+z}}\right)^2\left(\frac{\epsilon_B}{0.1}\right)^{1/2}\frac{E_{52}A_*^{1/2}}{\gamma_3\Delta_{10}}\ {\rm Jy}\ , \quad (51)$$

which is independent of time.

With the two characteristic frequencies (ν_{m3} and ν_c) and the peak flux ($F_{\nu_c,3}$) thus determined, we can now obtain the flux at any given frequency. We are particularly interested in the optical prompt emission, say, in the R band at $\nu_R = 4.5\times 10^{14}$ Hz, a frequency well above the cooling frequency ν_c but below the typical frequency ν_{m3} for typical parameters. In this spectral regime, we have (cf. Sari et al. 1998)

$$F_{\nu_R,3} = \left(\frac{\nu_R}{\nu_c}\right)^{-1/2}F_{\nu_c,3} = 14(1+X)\left(\frac{2-\sqrt{2}}{1+z-\sqrt{1+z}}\right)^2\times\left(\frac{\epsilon_B}{0.1}\right)^{-1/4}\frac{E_{52}^{5/4}\,t^{1/2}}{A_*^{1/2}\gamma_3\Delta_{10}^{5/4}}\ {\rm mJy}\ . \quad (52)$$

Note that in this case the optical flux increases with the square root of the observer's time, and a maximum is reached when the reverse shock crosses the inner edge of the freely coasting shell at the time

$$t_{\rm cr} = 10\,\frac{1+z}{2}\,\Delta_{10}\ {\rm s}\ . \quad (53)$$

The corresponding maximum flux is

$$F_{\nu_R,3}^{\max} = 46(1+X)\left(\frac{1+z}{2}\right)^{1/2}\left(\frac{2-\sqrt{2}}{1+z-\sqrt{1+z}}\right)^2\times\left(\frac{\epsilon_B}{0.1}\right)^{-1/4}\frac{E_{52}^{5/4}}{A_*^{1/2}\gamma_3\Delta_{10}^{3/4}}\ {\rm mJy}\ . \quad (54)$$

Interestingly, the peak flux is not sensitive to the magnetic energy fraction ϵ_B, one of the most uncertain parameters. Note that a flux density of 46 mJy in the R band corresponds to a magnitude of 12. Therefore, it is difficult to create a ninth-magnitude optical flash that lasts for several tens of seconds, as observed in GRB 990123 (Akerlof et al. 1999), in the reverse shock if the explosion occurs in a typical Wolf-Rayet wind, unless the parameters are far from typical, e.g., an explosion energy much higher than 10^{52} ergs (see § 4.3 for a discussion).

For completeness, we now discuss briefly the prompt, optical emission from the forward shock. The ambient medium shocked by the forward shock has the same cooling frequency ν_c as the shell material shocked by the reverse shock but a substantially higher typical frequency of

$$\nu_{m2} = \left(\frac{1}{1+z}\right)\frac{\gamma_{12}\gamma_{m2}^2 eB_{\rm tot}}{2\pi m_e c} = 5.7\times 10^{19}\left(\frac{3p-6}{p-1}\right)^2\left(\frac{1}{1+X}\right)^2\times\left(\frac{\epsilon_{e2}}{0.1}\right)^2\left(\frac{\epsilon_B}{0.1}\right)^{1/2}\frac{E_{52}^{1/2}}{\Delta_{10}^{1/2}\,t}\ {\rm Hz}\ , \quad (55)$$

where equation (42) is used to eliminate γ_{m2}. For typical parameters, we have $\nu_c < \nu_R < \nu_{m2}$, and the flux in the R band is given by

$$F_{\nu_R,2} = \left(\frac{\nu_R}{\nu_c}\right)^{-1/2}\frac{N_{e,2}(1+z)P_{\nu,\max}}{4\pi d_L^2}\ , \quad (56)$$

where the number of radiating electrons $N_{e,2}$ in the shocked ambient medium swept up by the forward shock increases linearly with time as

$$N_{e,2} = \left(\frac{1+X}{2}\right)\left(\frac{2}{1+z}\right)\frac{\dot{M}_w c\gamma_{12}^2\,t}{m_p V_w}\ . \quad (57)$$

Compared with the R-band flux for the reverse shock given in equation (52), the flux in the forward shock is down by a factor of

$$\frac{F_{\nu_R,2}}{F_{\nu_R,3}} = \frac{N_{e,2}}{N_{e,3}} = \frac{1}{2\xi^{1/2}} = \frac{1}{4.8}\,\frac{A_*^{1/2}\Delta_{10}^{1/2}\gamma_3}{E_{52}^{1/2}}\ . \quad (58)$$

Therefore, the optical flash is typically dominated by the reverse shock, as in the previously studied case of constant-density ambient medium.

After the coasting shell is completely shocked, the reverse-shock front disappears, and there is no more shell kinetic energy left to drive the forward shock. Instead of maintaining a constant Lorentz factor, the shocked region slows down with time as more ambient medium is swept up. The forward shock front begins to evolve as described in § 2. For the material in the reverse-shock region, we still have $\nu_c < \nu_{m3}$ at the time that the reverse shock disappears. The electrons in this region thus rapidly cool and do not con-

tribute to the emission, which is dominated by the forward shock region.

Synchrotron self-absorption may reduce our estimate of the optical prompt emission. A simple way to gauge this effect is to estimate the maximal flux emitted by the shocked shell material as a blackbody

$$F_{\nu,\rm bb} \approx (1+z)^3 \pi \left(\frac{R_\perp}{d_L}\right)^2 \left(\frac{2v^2}{c^2}\right) kT_{\rm eff} , \quad (59)$$

(Sari & Piran 1999b) with the observed size $R_\perp$ given roughly by

$$R_\perp \approx 2\gamma_{12}\, ct/(1+z) \quad (60)$$

and the effective temperature by

$$kT_{\rm eff} \approx \gamma_{12}\, \gamma_\nu m_e c^2/3 , \quad (61)$$

where γ_ν is the Lorentz factor of the electrons that radiate at the frequency ν and is given by $[2\pi(1+z)m_e c\nu/(\gamma_{12}\, eB_{\rm tot})]^{1/2}$. Substituting equations (60) and (61) into equation (59), we have

$$F_{\nu,\rm bb} \approx 1.5 \left(\frac{1+z}{2}\right)\left(\frac{2-\sqrt{2}}{1+z-\sqrt{1+z}}\right)^2 \times \left(\frac{\nu}{\nu_R}\right)^{5/2}\left(\frac{\epsilon_B}{0.1}\right)^{-1/4}\left(\frac{E_{52}^{3/4}\, t^{5/2}}{A_*\, \Delta_{10}^{3/4}}\right) {\rm mJy} , \quad (62)$$

which increases rapidly with time as $t^{5/2}$. At the particular time $t_{\rm cr}$ given in equation (53) when the reverse shock crosses the inner edge of the coasting shell, the blackbody flux is roughly

$$F_{\nu,\rm bb}^{cr} \approx 160 \left(\frac{1+z}{2}\right)^{7/2}\left(\frac{2-\sqrt{2}}{1+z-\sqrt{1+z}}\right)^2 \times \left(\frac{\nu}{\nu_R}\right)^{5/2}\left(\frac{\epsilon_B}{0.1}\right)^{-1/4}\left(\frac{E_{52}^{3/4}\, \Delta_{10}^{7/4}}{A_*}\right) {\rm mJy} , \quad (63)$$

which is roughly a factor of 3 above the (maximum) prompt optical flux at the same time, given by equation (54), for typical parameters. Therefore, it appears that synchrotron self absorption will not affect our estimate of the peak optical prompt emission from the reverse shock significantly, unless γ_3 and/or Δ_{10} are unusually small, and/or A_* and/or E_{52} are exceptionally large. Finally, we note that the prompt emission estimated here may also be lowered by inverse Compton scattering, which cools the radiating electrons in addition to synchrotron emission (Sari & Piran 1999b)

3.2. *Comparison with the ISM Case*

Prompt emission from gamma ray bursts in a constant-density interstellar medium has been investigated in detail by Sari & Piran (1999a, 1999b) and Mészáros & Rees (1999). For the ease of comparison, we shall compute several key quantities of the reverse shock, using the same notations and under the same assumptions as the wind case. We limit our discussion to the case of a relativistic reverse shock, which demands that the relative Lorentz factor between the shocked and unshocked shell materials,

$$\gamma_{34} = 1.5 \left(\frac{2}{1+z}\right)^{1/4} \frac{\gamma_3\, n^{1/8}\Delta_{10}^{1/8}\, t^{1/4}}{E_{52}^{1/8}} , \quad (64)$$

be greater than unity. We assume that the shell γ_3 is large enough (typically of order unity) so that the reverse shock becomes relativistic a few seconds after the explosion. The quantity n in the above equation is the number density of the ambient medium in units of cm^{-3}.

The Lorentz factor for the forward shock is much higher. We find

$$\gamma_{12} = 320 \left(\frac{1+z}{2}\right)^{1/4} \frac{E_{52}^{1/8}}{n^{1/8}\Delta_{10}^{1/8}\, t^{1/4}} , \quad (65)$$

which decreases gradually with time. To account for the deceleration, we have adopted a relation between the observer's time t and the time T in the rest frame of the origin of $t = (1+z)T/(4\gamma_{12}^2)$ instead of equation (46). Assuming a purely hydrogenic interstellar medium (with $X = 1$), we obtain a typical frequency in the reverse shock of

$$\nu_{m3} = 1.6 \times 10^{14} \left(\frac{3p-6}{p-1}\right)^2 \left(\frac{2}{1+z}\right) \times \left(\frac{\epsilon_{e3}}{0.1}\right)^2 \left(\frac{\epsilon_B}{0.1}\right)^{1/2} \gamma_3^2\, n^{1/2} \ {\rm Hz} \quad (66)$$

and a cooling frequency of

$$\nu_c = 1.6 \times 10^{17} \left(\frac{\epsilon_B}{0.1}\right)^{-3/2} \frac{\Delta_{10}^{1/2}}{E_{52}^{1/2}\, nt} \ {\rm Hz} . \quad (67)$$

For typical parameters, we therefore have $\nu_{m3} < \nu_R < \nu_c$, and the flux density in the R band is given approximately by

$$F_{\nu_R,3} = \left(\frac{\nu_{m3}}{\nu_R}\right)^{(p-1)/2} F_{\nu_m,3} = 85 \left(\frac{\nu_{m3}}{\nu_R}\right)^{(2p-5)/4} \left(\frac{2}{1+z}\right)^{1/4} \times \left(\frac{2-\sqrt{2}}{1+z-\sqrt{1+z}}\right)^2 \left(\frac{3p-6}{p-1}\right)^{3/2} \left(\frac{\epsilon_{e3}}{0.1}\right)^{3/2} \times \left(\frac{\epsilon_B}{0.1}\right)^{7/8} \frac{\gamma_3^{1/2}\, n^{5/8} E_{52}^{5/4}\, t^{1/2}}{\Delta_{10}^{5/4}} \ {\rm mJy} , \quad (68)$$

where we have used equations (48)–(49) to derive the peak flux density, $F_{\nu_m,3}$, at the typical frequency.[3] The factor involving the ratio

$$\frac{\nu_{m3}}{\nu_R} = 0.36 \left(\frac{2}{1+z}\right)\left(\frac{3p-6}{p-1}\right)^2 \left(\frac{\epsilon_{e3}}{0.1}\right)^2 \left(\frac{\epsilon_B}{0.1}\right)^{1/2} \gamma_3^2\, n^{1/2} \quad (69)$$

in equation (68) becomes unity for the canonical value of $p = 2.5$. Note that the optical flux density increases with time as $t^{1/2}$, as in the wind case. For typical parameters, it appears that the optical flux in the ISM case is higher than that in the wind case (by a factor of about 6), and the emission peaks at a magnitude of about 10 when the reverse shock crosses the inner edge of the freely coasting shell. Of course, other choices of parameters can change these numbers substantially. For example, if one adopts a shell Lorentz factor $\gamma_{\rm sh}$ of 300 instead of 10^3, then the optical

[3] We note here that the peak flux would be lower by a factor of about 3 if the formalism of Wijers & Galama (1999) is adopted.

fluxes in the wind and ISM cases would become nearly identical, both peaking at a magnitude of about 10.7. Note that the prompt optical fluxes in the wind and ISM cases have the same dependence on the energy E_{52}, the shell width Δ_{10}, and time t. They have opposite dependences on the shell Lorentz factor γ_3, the ambient density, and the magnetic energy fraction ϵ_B. Furthermore, whereas the optical flux in the ISM case increases fairly rapidly with the electron energy fraction ($\propto \epsilon_e^{3/2}$ if $p = 2.5$), that in the wind case is independent of ϵ_e.

The X-ray emission from the reverse shock of the wind case is expected to be higher than that in the ISM case. For definitiveness, we consider the emission at 2 keV, with $\nu_X = 4.8 \times 10^{17}$ Hz. In the wind case (with $X = 0$), we have for typical parameters $\nu_c < \nu_X < \nu_{m3}$ and an X-ray flux density of

$$F_{\nu_X,3} = 440\left(\frac{2-\sqrt{2}}{1+z-\sqrt{1+z}}\right)^2\left(\frac{\epsilon_B}{0.1}\right)^{-1/4} \times \frac{E_{52}^{5/4}\, t^{1/2}}{A_*^{1/2}\gamma_3\,\Delta_{10}^{5/4}}\ \mu\mathrm{Jy}\ , \quad (70)$$

which increases with time as $t^{1/2}$. For typical parameters, it has a peak value of 1.4 mJy when the reverse shock crosses the inner edge of the freely coasting shell. It is interesting to note that the peak value is comparable to the flux density observed in GRB 970228 and GRB 970508, two of the GRBs to be discussed in detail in § 4, on the timescale of tens of seconds, which is roughly 10 keV cm^{-2} s^{-1} (or about 3 mJy at 2 keV; see Figs. 1 and 2 of Frontera et al. 2000). The prompt X-ray emission from the forward shock should be weaker, as in the case of prompt optical emission. Therefore, the prompt X-ray emission in the wind case does not appear to violate any observational constraints. Indeed, for some GRBs, it may be able to account for at least part of the early X-ray emission detected by the Wide Field Camera of the *BeppoSAX*. We shall explore this possibility elsewhere.

In the ISM case, we have for typical parameters $\nu_{m3} < \nu_c < \nu_X$ instead, and an X-ray flux density of (assuming $p = 2.5$)

$$F_{\nu_X,3} = 260\left(\frac{2}{1+z}\right)^{1/4}\left(\frac{2-\sqrt{2}}{1+z-\sqrt{1+z}}\right)^2 \times \left(\frac{\epsilon_{e3}}{0.1}\right)^{3/2}\left(\frac{\epsilon_B}{0.1}\right)^{1/8}\frac{\gamma_3^{1/2}\, n^{1/8} E_{52}}{\Delta_{10}}\ \mu\mathrm{Jy}\ , \quad (71)$$

which is independent of time and is a factor of about 5 lower than the peak flux in the wind case for typical parameters. The contrast in prompt X-ray flux between the wind and ISM cases would be higher if a smaller shell Lorentz factor $\gamma_{\rm sh}$ is adopted, keeping other parameters at their typical values.

4. OBSERVED SOURCES

4.1. *GRB 970228*

A recent development is the finding of evidence for a supernova in GRB 970228 (Reichart 1999; Galama et al. 2000); the late spectrum is especially convincing. At first sight, this appears to be in conflict with the apparently interstellar nature of the afterglow: Fruchter et al. (1999b) found time evolution with $\alpha = -1.10 \pm 0.05$ at optical wavelengths, and the overall evolution appears to be compatible with expansion in a constant-density medium (Wijers et al. 1997). However, if the late observations are attributed to a supernova, the decline of the nonthermal optical afterglow steepens and $\alpha = -1.58 \pm 0.28$ (Reichart 1999) or $\alpha = -1.73^{+0.09}_{-0.12}$ (Galama et al. 2000). With a plausible amount of extinction, Reichart (1999) finds $\beta = -0.61 \pm 0.32$ at optical wavelengths. The optical-to-X-ray spectral index is better constrained; Galama et al. (2000) find $\beta_{\rm ox} = -0.780 \pm 0.022$ at early times. Cooling evolution (ν_c below optical wavelengths) is unlikely because $\beta = -0.78$ would imply $p = 1.56$. With $\beta = -0.78$, an adiabatic blast wave in a constant-density medium implies $\alpha = -1.17$, but a blast wave in a wind implies $\alpha = -1.67$ (Mészáros et al. 1998; CL), in good agreement with the observed decline. GRB 970228 can thus be plausibly added to the wind interaction category with $p \approx 2.6$.

The evolution of the X-ray afterglow shows $\alpha = -1.33^{+0.11}_{-0.13}$, $\beta = -0.96 \pm 0.19$ up to day 4 at 2–10 keV (Costa et al. 1997) and $\alpha = -1.50^{+0.35}_{-0.23}$ up to day 10 at 0.1–2.4 keV (Frontera et al. 1998). There is some evidence for a flatter rate of decline at X-ray frequencies compared to the optical, which would suggest that ν_c is below the X-ray regime. Equation (25) shows that the X-ray emission should be in the cooling regime during the observed time period for reasonable values of the parameters. The spectrum may be somewhat flatter than $\beta = -0.78$ in the optical, steepening to $\beta < -1$ in the X-ray regime.

GRB 970228 was monitored at radio wavelengths but was not detected at limits between 10 μJy and 1 mJy over the first year (Frail et al. 1998a). In an interstellar interaction model, the peak flux, $F_{\nu,\rm max}$, should remain constant and move to lower frequency with time. Wijers et al. (1997) take $F_{\nu,\rm max} \approx 5$ mJy based on the X-ray flux near the end of the initial γ-ray burst. The radio emission clearly did not reach this peak flux. Frail et al. (1998a) explain this result by claiming that $F_{\nu,\rm max}$ for the afterglow could not be estimated from the initial burst and that $F_{\nu,\rm max} \approx 20$–$40$ μJy. This requires a substantial gap in the X-ray evolution between the initial burst and the afterglow and that the first optical observations have occurred shortly after ν_m passed through optical wavelengths. In a wind model, $F_{\nu,\rm max} \propto t^{-1/2}$, so there is a drop in $F_{\nu,\rm max}$ from the time of the early X-ray observations ($t \approx 50$ s) to the time of the radio observations. The radio limits can be accommodated even with an initially high X-ray flux in the afterglow.

4.2. *GRB 970508*

The optical afterglow of GRB 970508 followed power-law evolution from day 2 to day $\gtrsim 100$ with $\alpha = 1.141 \pm 0.014$ (Galama et al. 1998b). Galama et al. (1998a) compiled the radio to X-ray spectrum of the source on day 12.1 (see also Wijers & Galama 1999). They estimated that the cooling frequency was at $\nu_c = 1.6 \times 10^{14}$ Hz or a wavelength of 2 μm, i.e., a frequency just below optical frequencies. Based on the day 12.1 spectrum, Galama et al. (1998a) estimate that $p = 2.2$, which yields $\alpha = -1.15$ and $\beta = -1.1$ for $\nu > \nu_c$ in both the $s = 0$ and $s = 2$ cases. The value of p is supported by both the observed spectrum and the rate of decline. However, because of the similar optical and X-ray evolution for ISM and wind interaction, radio observations are crucial for distinguishing between the $s = 0$ and $s = 2$ cases. Extensive radio data exist for GRB 970508, at 8.46, 4.86, and 1.43 GHz frequencies (Frail et al.

1997; Galama et al. 1998c; Waxman et al. 1998; Frail, Waxman, & Kulkarni 2000a). Here, we fit these radio data using the thin shell model of Li & Chevalier (1999) to determine the burst parameters. Our model treats synchrotron emission from a (trans-) relativistic blast wave propagating in an r^{-2} medium. Synchrotron self-absorption and relativistic effects are included, but not cooling. As usual, we take a power-law distribution of electron energy and adopt an energy index of $p = 2.2$.

Since the observed radio frequencies are all below the cooling frequency ν_c in the time interval of interest, fitting the radio data alone fixes only three of four parameters, as discussed in Li & Chevalier (1999). The additional constraint comes from the observed flux in the R band, which is affected by cooling. Together, we find the best model parameters to be: $\epsilon_e = 0.2$, $\epsilon_B = 0.1$, $E_{52} = 0.3$, and $A_* = 0.3$ (which is in the expected range of a Wolf-Rayet star). The model fit is displayed in Figures 2 and 3; the radio data, from the VLA (Frail et al. 2000a), and the model are the same in the two figures and are shown in two different ways for clarity. The general evolution shown in the numerical model is along the lines of model D in § 2.4, but it has gradual transitions between the evolutionary phases. This is due both to the smoothness of the transitions in the radio spectrum and to the time lag effects, which result in different parts of the shell being observed at different evolutionary phases at the same observer's time.

The initial rise of the model flux at 1.43 GHz has $F_\nu \propto t$, as expected in the self-absorbed regime. The model flux on day 6.2 does fall below the 1.43 GHz VLA observation of 100 ± 30 μJy (Frail et al. 2000a). However, monitoring at Westerbork at 1.4 GHz over the first 40 days failed to detect the afterglow (Galama et al. 1998c). The Westerbork observations have lower sensitivity than those at the VLA, but a combined map of the 21 observations during this time period yielded a flux of 33 ± 40 μJy. Galama et al. (1998c) take this as evidence that the source is well into the self-absorbed regime at early times, as it is in our model.

Both wind and interstellar relativistic spherical models predict that $\nu_m \propto t^{-3/2}$, and the data over the range 1.4–86 GHz are in approximate accord with this expectation (Frail et al. 2000a). However, the models differ in that F_{ν_m} decreases with time in the wind case but not in the interstellar case. Figure 3 shows that the observed decrease of F_{ν_m} is well reproduced by the wind model. Additional data are available at 15 and 86 GHz, and Frail et al. (2000a) find that $F_{\nu_m} \propto \nu_m^{0.40 \pm 0.04}$, close to the expectation of $F_{\nu_m} \propto \nu_m^{0.33}$ in the wind model.

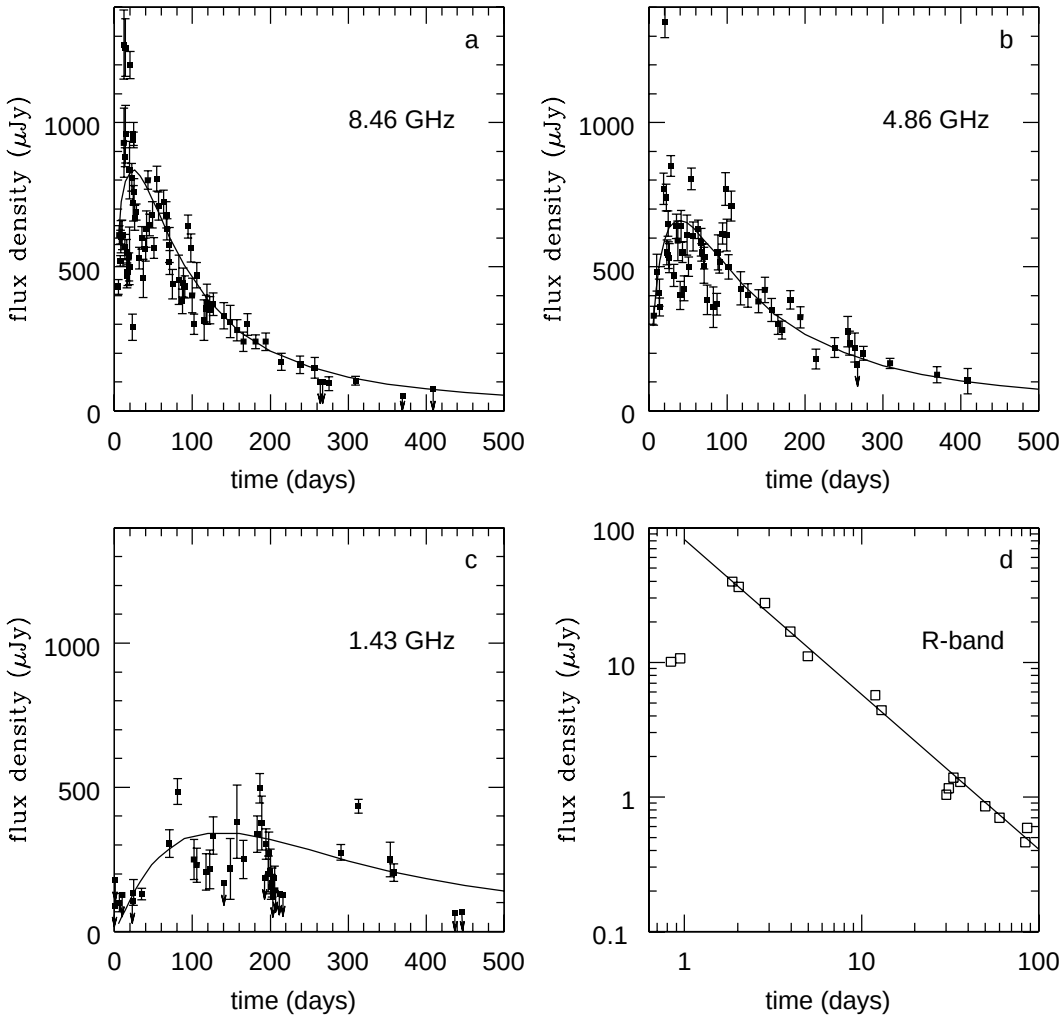

FIG. 2.—Wind interaction model for the afterglow of GRB 970508. Radio data are taken from Frail et al. (1997, 2000a). R-band data are taken from Sokolov et al. (1998). The best model fit parameters are listed in the text.

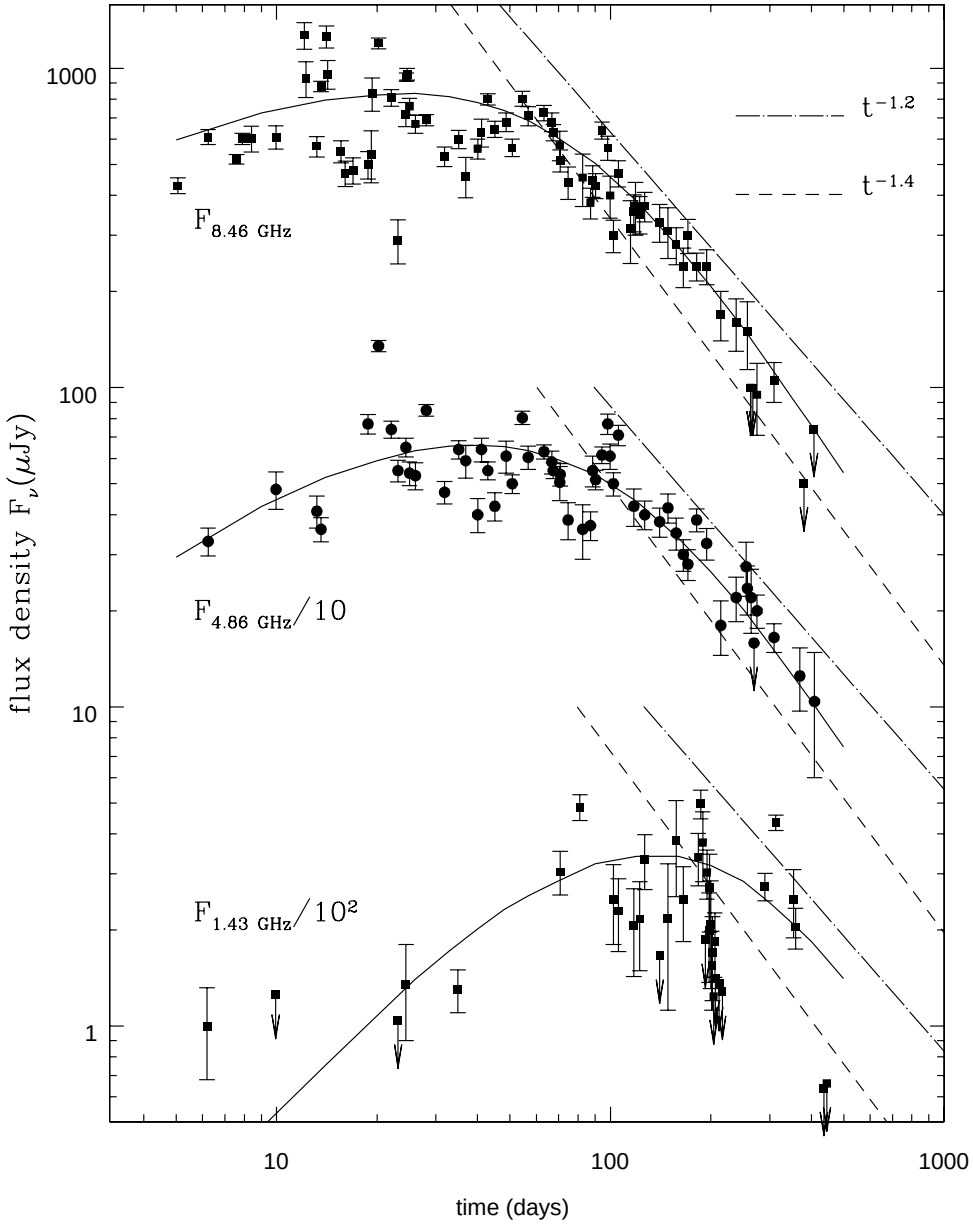

FIG. 3.—A log-log plot of the same observed data and model fits at the radio frequencies as in Figure 2, showing the curvature in the power-law flux decay after about day 100. The data and fits for 4.86 GHz and 1.43 GHz are artificially lowered by factors of 10 and 10^2, respectively, for clarity.

After about day 100, the 4.86 and 8.46 GHz fluxes tend toward approximate power-law declines (Fig. 2; Frail et al. 2000a). Frail et al. (2000a) find that for $t > 90$ days, $\alpha_{8.46\mathrm{GHz}} = -1.3 \pm 0.1$ and $\alpha_{4.86\mathrm{GHz}} = -1.1 \pm 0.1$ and that the data at the two frequencies can be combined for $t > 110$ days to yield $\alpha = -1.14 \pm 0.06$ and $\beta = -0.50 \pm 0.06$ (where $F_\nu \propto t^\alpha \nu^\beta$). They suggest that "$\beta$ undergoes an abrupt drop from positive to negative values" at $t \approx 100$ days. Our model does not produce an abrupt drop in β, but we believe that the data are consistent with a gradual change (see Fig. 3). We attribute the fact that $\alpha_{4.86\mathrm{GHz}}$ is deduced to be larger than $\alpha_{8.46\mathrm{GHz}}$ to the later transition from flat evolution at the lower frequency. Figure 3 shows that the model light curve behavior does go to $F_\nu \propto t^{-1.4}$, as expected for relativistic, spherical, adiabatic expansion in a wind with $p = 2.2$, but that it eventually becomes steeper. The steepening is due to a transition to nonrelativistic expansion, which is included in our numerical model (Li & Chevalier 1999). At $t = 400$ days, equation (5) yields $\gamma = 1.2$ for the low-frequency case.

The determination of ν_c was carried out as follows. Approximately, the observed late time flux decline at 8.46 GHz follows

$$F_{8.46\ \mathrm{GHz}} \approx 500\left(\frac{t}{100\ \mathrm{days}}\right)^{-1.4}\ \mu\mathrm{Jy}\ , \qquad (72)$$

which implies a flux in the R band (with $\nu_R = 4.5 \times 10^{14}$ Hz) of

$$F_R = \left(\frac{8.46 \times 10^9}{4.5 \times 10^{14}}\right)^{0.6} F_{8.46\ \mathrm{GHz}} \approx 0.73\left(\frac{t}{100\ \mathrm{days}}\right)^{-1.4}\ \mu\mathrm{Jy} \qquad (73)$$

if the R band frequency is below the cooling frequency ν_c. The cooling frequency is estimated in equation (14), which, for the inferred parameters, becomes

$$\nu_c \approx 1.4 \times 10^{13} t_{\rm days}^{1/2} \ {\rm Hz} \ . \tag{74}$$

Setting $\nu_c = \nu_R$, we obtain a cooling time $t_R = 1000$ days for the R-band emission. After t_R, $\nu_R > \nu_c$, and the R-band flux is given by equation (73). Before t_R, we have $\nu_R < \nu_c$, and the R-band flux is given instead by

$$F_R = 0.73 \left(\frac{t_R}{100 \ {\rm days}} \right)^{-1.4} \left(\frac{t}{t_R} \right)^{-1.15} = 82 t_{\rm days}^{-1.15} \ \mu{\rm Jy} \ . \tag{75}$$

This expected flux is shown in Figure 2*d*. Our model fits are reasonable overall in all four frequencies, lending support to the wind interaction scenario for this GRB. X-ray observations are expected to be compatible with our model because it is the same as an ISM model for $\nu > \nu_c$. The evolution between 6 hr and 6 days can be approximately fitted by $F_\nu \propto t^{-1.1 \pm 0.1}$ (Piro et al. 1998), and the optical/X-ray spectral index is compatible with $\beta_{\rm ox} = -p/2 = -1.1$ (Galama et al. 1998a).

Galama et al. (1998a) end their paper advocating an $s = 0$ blast-wave model for GRB 970508 by describing three deficiencies of the model: (1) $F_{\nu,\rm max}$ should be constant but is observed to decrease with time; (2) ν_A is predicted to be time independent but is observed to decrease with time, and the rise of the radio fluxes is slower than expected; and (3) the decay after maximum at mm wavelengths is perhaps somewhat faster than expected. All of these problems are addressed by the wind model, which provides approximate quantitative agreement with the observations. Waxman et al. (1998) also noted the problems with a relativistic, spherical, $s = 0$ model and suggested jet effects and a transition to nonrelativistic expansion as possible solutions. Frail et al. (2000a) developed these suggestions in more detail and proposed three phases of evolution in a uniform density medium: (1) $2 < t < 25$ days: relativistic expansion in which the evolution appears spherical (although it is a jet) because relativistic effects allow only a part of the flow to be observed; (2) $25 < t < 100$ days: jet spreading, causing F_{ν_m} and the radio fluxes to drop below what would be obtained in an extension of phase 1; and (3) $100 < t < 450$ days: nonrelativistic, spherical expansion after jet spreading is complete. Frail et al. (2000a) show that the emission expected in phase 3 is consistent with the radio data, but the complete model has yet to be calculated. Relativistic time lag effects are likely to be significant at transition times, and a possible concern is that the optical light curve does not clearly show evidence for the transition from phase 1 to phase 2.

Although the radio data appear to provide support for the wind model, the wind interpretation does give rise to possible problems regarding synchrotron cooling. In the wind model, ν_c increases with time; at optical wavelengths, a transition is expected from cooling evolution to adiabatic evolution. The opposite is true in $s = 0$ models. Galama et al. (1998a) cite evidence that ν_c evolves as expected in an $s = 0$ model. They identify an observed optical spectral transition between 1.0 and 1.8 days from $\beta = -0.54 \pm 0.14$ to $\beta = -1.12 \pm 0.04$ with the break frequency ν_c passing through the R_C band. The wind model would predict cooling in the R_C band at this early time and no transition. However, in the time before day 1.5, the observed light curve deviates strongly from standard afterglow models (e.g., Galama et al. 1998b; Fruchter et al. 1999c), so the early spectral index cannot be used as a constraint on models for the later power-law evolution. Galama et al. (1998a) also cite moderately flat spectra between the K band (Chary et al. 1998) and the R_C band on days 4.3 and 7.3 as supporting adiabatic evolution in the infrared at that time. This is in conflict with the wind model, but we believe that the overall weight of evidence supports the wind model. In fact, Chary et al. (1998) find that their data are consistent with a $t^{-1.2}$ decline and state that their data "agree reasonably well" with a spectral index about -1, as found in the optical (and expected in our model). In the wind model, the optical spectrum should flatten and the light curve should steepen at late times.

Our model fails to account for the optical evolution before day 2 (e.g., Galama et al. 1998b; Fruchter et al. 1999c). At early times, the blast wave is expected to be in the fast cooling regime ($\nu_m > \nu_c$); this occurs at 500 s in the $s = 0$ model (Galama et al. 1998a) but at ~ 1 day in the wind model. Although the sharp rise in the light curve may be related to this transition, it is not possible to account for the rise in a straightforward way. In addition, Piro et al. (1999) have found possible evidence for redshifted iron line emission in the X-ray afterglow at an age ~ 1 day. In our model, the preshock density at that age is $\sim 1 \times 10^{-23}$ g cm^{-3}, which is orders of magnitude smaller than the density required for the line feature (Piro et al. 1999). As noted by Piro et al. (1999), ordinary stellar mass loss cannot account for the feature that they tentatively observe.

One expectation of the wind interaction model is that the event be accompanied by a supernova. However, Fruchter (1999) has found that a supernova such as SN 1998bw added to the power-law decline of the nonthermal afterglow emission would give an observable bump in the light curve at $t \sim 20$–50 days. Such a bump is not seen (Fruchter et al. 1999c), and a supernova in GRB 970508 would have to be about 1 mag fainter than SN 1998bw (Fruchter 1999). Considering possible differences in ejected mass, ^{56}Ni mass, and explosion energy, we believe that some variation in supernova properties is plausible.

A remarkable property of our model is that it approximately reproduces the radio light curves over the entire range of observations from ages of 5 to 400 days. There are reasons why deviations from the model might be expected. If the ejecta initially cover a small solid angle, steepening of the light curve is expected as the blast wave slows down and there is eventually lateral expansion (§ 2.6). Equation (31) shows that $\theta_0 \gtrsim 1$ is required to avoid the steepening; that is, the blast wave is spherical or nearly so. Rhoads (1999) and Sari et al. (1999) reached a similar conclusion for GRB 970508 based on an interstellar interaction model for the optical emission from the source. In addition, the blast wave must remain within the steady stellar wind. From equation (4) and the blast-wave parameters, the observed shock has $R \approx 3 \times 10^{18}$ cm. The discussion in CL shows that the wind can plausibly extend to this distance.

4.3. *GRB 990123*

The afterglow of GRB 990123 was briefly discussed by CL as a probable case of ISM interaction. The observations over the time period 0.01–1.5 day (Kulkarni et al. 1999; Galama et al. 1999; Castro-Tirado et al. 1999) can be fitted

by an ISM interaction model with $p = 2.5$ and optical wavelengths in the adiabatic regime ($\alpha = -1.12$; $\beta = -0.75$) and X-ray wavelengths in the cooling regime ($\alpha = -1.38$; $\beta = -1.25$). The observed steeper decline in the X-rays versus the R band ($\alpha_X = -1.44 \pm 0.07$ vs. $\alpha_R = -1.10 \pm 0.03$; Kulkarni et al. 1999) is expected for ISM interaction but not for wind interaction.

A new feature observed in GRB 990123 was a ninth magnitude optical flash overlapping with the GRB (Akerlof et al. 1999). Sari & Piran (1999a) and Mészáros & Rees (1999) found that the properties of the optical emission over the first ~ 15 minutes could be modeled by synchrotron emission from the reverse-shock front resulting from interaction with a constant-density interstellar medium. In § 3 here, we find it difficult to produce such a strong synchrotron, optical flash with standard parameters. If we let $z = 1.6$, $X = 0$, and $\Delta_{10} = 4$ (so that the emission peaks around 50 s, as observed) and assume $A_* = \gamma_3 = 1$ and $\epsilon_B = 0.1$, then an explosion energy of 5×10^{53} ergs is required to produce the ninth magnitude optical flash. Such an energy is nearly 2 orders of magnitude higher than the standard value, but it is not a problem for GRB 990123, the brightest γ-ray burst with a well-localized position. The estimated isotropic γ-ray energy alone for this source is $\sim 3 \times 10^{54}$ ergs (Kulkarni et al. 1999). The explosion energy could be higher. Therefore, the magnitude of the optical flash does not provide a clear discriminator between wind interaction and interstellar interaction in this case.

The observed temporal behavior of the optical flash of GRB 990123 is not compatible with the predictions of the wind interaction model. The flash is predicted to rise with time as $t^{1/2}$ (assuming that self-absorption is not significant, which is true for the parameters listed in the preceding paragraph), whereas the observed rise is much steeper, close to $t^{3.7}$ evolution.[4] In addition, the emission from the reverse shock is short lived in a wind interaction model and is not compatible with the observed t^{-2} flux evolution over the first 15 minutes (Akerlof et al. 1999; Sari & Piran 1999a; § 3). The reason for the cutoff of the emission in the wind case is that $\nu_c < \nu_m$, so once the reverse-shock front passes through the shell the electrons rapidly cool and there is no more emission from the reverse shock. In the ISM case, $\nu_c > \nu_m$ and long-lived emission with a power-law decline can occur (Sari & Piran 1999a).

4.4. *GRB 990510*

The optical afterglow of GRB 990510 was well observed in the first 4 days after the burst (Stanek et al. 1999; Harrison et al. 1999). The light curve could be well fitted by an initial power law $F_\nu \propto t^{\alpha_1}$ followed by a steepening to another power law $F_\nu \propto t^{\alpha_2}$. Although there was considerable overlap in the data that they used for their analyses, Stanek et al. (1999) found $\alpha_1 = -0.76 \pm 0.01$ and $\alpha_2 = -2.40 \pm 0.02$ while Harrison et al. (1999) found $\alpha_1 = -0.82 \pm 0.02$ and $\alpha_2 = -2.18 \pm 0.05$. The initial flat evolution is strongly suggestive of adiabatic evolution ($\nu_m < \nu < \nu_c$) in a constant-density medium ($F_\nu \propto t^{-3(p-1)/4}$). The initial decline rate measured by Harrison et al. (1999) is then consistent with $p = 2.1$ and with the later evolution being due to a slowed jet with $F_\nu \propto t^{-p}$ (Sari et al. 1999). The results of Stanek et al. (1999) suggest a somewhat smaller value of p from the early evolution and a somewhat larger value of p from the later evolution, but they are close to the expected evolution. The value $p = 2.1$ implies $F_\nu \propto \nu^{-0.55}$, which is consistent with the spectrum $F_\nu \propto \nu^{-0.61 \pm 0.12}$ measured from *BVRI* photometry (Stanek et al. 1999). The hypothesis of jet evolution is supported by radio data, which are consistent with the expected $F_\nu \propto t^{-1/3}$ evolution (Harrison et al. 1999).

Evolution in a constant-density medium thus gives a consistent picture for this afterglow. Evolution in a wind cannot plausibly account for the early flat decline, even taking into account the possibility of being in the strong cooling regime (§§ 2.2 and 2.3).

The steepening of the afterglow light curve to $\alpha_2 = -2.2$ after 1.4 days should have facilitated the observation of a supernova above the nonthermal emission. Our model would predict the absence of such a supernova if it was an interstellar interactor, but a test is difficult because of the high redshift of the event, $z = 1.619$ (Vreeswijk et al. 1999). *HST* observations by Fruchter et al. (1999a) showed that on 1999 June 17.9 (day 38.5) the afterglow flux was somewhat above the extrapolation of the t^{α_2} decline, but the excess counts were a factor 7 below what would be expected if a supernova such as SN 1998bw were present.

4.5. *Discussion*

A summary of the results from this section is in Table 1. In addition to the sources discussed here, we have added GRB 980425 (Kulkarni et al. 1998; Li & Chevalier 1999) and GRBs 980326 and 980519 (CL). The redshift is given in column (2) for those for which it has been determined (see the recent compilation of Ghisellini 1999 for references). The next column gives the afterglow type, as determined by the afterglow evolution. We claim that GRBs 970228 and 970508 are probable wind interactors, although they have been widely interpreted in terms of interstellar interaction in the literature. The reasons for this are varied. In the case of GRB 970228, the recognition of supernova emission in the optical light curve yields a steeper nonthermal afterglow decline, in line with expectations for wind interaction. In the case of GRB 970508, the cooling frequency ν_c is somewhat below optical wavelengths, so the high-frequency evolution is the same for wind and interstellar interaction. However, the predicted evolution is different at radio wavelengths, and the radio data are compatible with wind interaction. The radio data are crucial for typing this burst, and they are suggestive of wind interaction for the afterglow of GRB 980519.

Although we believe that the radio data for GRB 970508 support a wind interaction model, this is a controversial result. Frail et al. (2000a) have proposed a uniform medium interaction model, as discussed in § 4.2. In addition, the high-frequency, steeply declining afterglows of GRBs 980326 and 980519 can be interpreted in terms of jet evolution (Sari et al. 1999). If the jet model applies, either wind or interstellar interaction could have taken place (see § 2.6). Detailed observations over a long time base are needed to clearly discriminate between wind and interstellar interaction models.

In a paper that appeared after this paper was submitted, Livio & Waxman (2000) addressed the problem of dis-

[4] We note here that the steep rise is not reproduced in the simplest ISM case with a uniform freely coasting shell and a relativistic reverse shock either. To explain the steep rise, one needs to take into account additional complications, such as a nonuniform coasting shell or a transrelativistic reverse shock.

TABLE 1

PROPERTIES OF GRB AFTERGLOWS

Burst GRB (1)	Redshift z (2)	Afterglow Type (3)	Spectral Index, p (4)	Supernova like SN 1998bw (5)	Prompt, Bright Optical Flash (6)	Jet (7)
970228.....	0.695	Wind	2.6	Yes	...	...
970508.....	0.835	Wind	2.2	No	...	No
980326.....	...	Wind	3.0	Yes	...	...
	...	Jet	2.2	Yes	...	Yes
980425.....	0.0085	Wind	2.5	Yes	...	No
980519.....	...	Wind	3.0	No	...	...
	...	Jet	2.2	No	...	Yes
990123.....	1.60	ISM	2.5	...	Yes	Yes
990510.....	1.619	ISM	2.1	No	...	Yes

tinguishing wind and interstellar interaction afterglows when jets are present. They note that once the lateral jet expansion is complete, spherical, subrelativistic expansion is expected (see § 2.5). This should lead to a flattening of the afterglow light curves. If the steep decline of some afterglows is due to spherical wind interaction and not to jet interaction, flattening of the light curve would not occur unless the blast-wave shock front reached the edge of the free wind expansion region.

We have examined the data available on other sources but have not found more that can be typed. The afterglow of GRB 971214 was extensively observed at optical wavelengths, but there is probably significant extinction in the host galaxy and radio data are not available. The afterglow of GRB 980329 was observed at radio wavelengths; the 8.3 and 4.9 GHz data of Taylor et al. (1998) over the first 30 days appear to be in the self-absorbed regime. The data appear to be better approximated by $F_\nu \propto t^{1/2}$ evolution (interstellar) as opposed to $F_\nu \propto t$, but there are strong scintillation effects. The higher frequency data are difficult to model. Dai & Lu (1998) suggested that GRB 970616 is a wind interactor based on the steep decline with time indicated by two X-ray flux measurements; we believe that more detailed observations are needed to make an identification.

Column (4) of Table 1 shows that the estimated electron energy spectral index, p, varies over the set of bursts. The probable error in these estimates, ~ 0.1, cannot account for the range. The high values of p for GRBs 980326 and 980519 are reduced in jet models for these sources (Sari et al. 1999), but a range in p of at least ~ 2.1–2.5 is difficult to avoid. The lack of a universal value for p calls into question the initial assumption that the shock front accelerates electrons to a power law above γ_m that is constant with energy and with time. The possibility of curvature in the spectrum and/or time evolution of p should be examined as the data on GRB afterglows improve.

Column (5) indicates whether there is evidence for a supernova such as SN 1998bw in the emission from the source. The case is clearest for GRB 980425 and its probable association with SN 1998bw. The data on GRB 970228 are compatible with a supernova very much like SN 1998bw (Reichart 1999; Galama et al. 2000). This is also true for GRB 980326, although the observational case is not as clear (Bloom et al. 1999b). As discussed in § 4.2, GRB 970508 does not show evidence for a supernova such as SN 1998bw. Bloom (1999) has reported a similar situation for GRB 980519. These facts appear to contradict the expectations of our model. However, in both cases a supernova somewhat fainter than SN 1998bw can be accommodated. Supernovae associated with GRBs can be expected to have a range of properties; some variation in explosion energy, ejected mass, and mass of ^{56}Ni are all plausible.

Column (6) lists whether a prompt, optical flash was observed. Such an event has been seen only in GRB 990123 and was attributed to synchrotron emission from the reverse-shock wave (Sari & Piran 1999a; Mészáros & Rees 1999). In our picture, the optical synchrotron emission from the reverse-shock wave of bursts with a wind-type afterglow could have a magnitude comparable to but would die off faster than bursts with an interstellar-type afterglow. The decay rate of the optical flash in GRB 990123 is consistent with an ISM type, not with a wind type.

The last column of Table 1 lists whether there is evidence for a jet in the afterglow evolution. The entry "No" indicates that the jet opening angle is $\theta_0 \gtrsim 1$. The case of GRB 970508 was discussed by Rhoads (1999) and Sari et al. (1999) for ISM interaction and in § 4.2 for wind interaction. Li & Chevalier (1999) found that semirelativistic, spherically symmetric models provided a good description of SN 1998bw/GRB 980425. GRBs 990123 and 990510 show probable jet effects on a timescale ~ 1–2 days (Kulkarni et al. 1999; Harrison et al. 1999; Sari et al. 1999). The cases of GRBs 980326 and 980519 are controversial. If the steep declines of their optical afterglows are interpreted as jet effects (Sari et al. 1999) then the jet effects occur at an earlier time than for GRBs 990123 and 990510, but if the declines are interpreted as wind interaction (CL) then the jet effects occur later if at all.

5. TWO TYPES OF PROGENITORS

In CL, we suggested that there are two types of GRB progenitors among the well-observed sources: massive stars that have afterglows characteristic of wind interaction and are likely to be accompanied by supernovae and compact binary mergers that have afterglows characteristic of constant-density interstellar interaction and are not accompanied by supernovae. Our discussion here has increased the wind group by adding GRBs 970228 and 970508. The pattern of association with a supernova is strengthened by the finding of strong evidence for a supernova in GRB 970228. A new result here is that the prompt optical flash in a wind interaction GRB is expected to rise slowly and to disappear abruptly, in contrast to the observed temporal behavior of the optical flash of GRB 990123. The contradiction points to an interstellar interaction for this case, which

supports the interpretation of the afterglow light curve evolution by CL.

Another possible indicator of the GRB progenitor type is the location in a galaxy (Paczyński 1998). For the cases in which imaging with *HST* is available, the bursts appear to be superposed on or near the optical disks of the host galaxies. In the case of GRB 990123, the burst is at about 5.8 kpc (0".67) from the center of the host galaxy, near the edge of the optical disk (Bloom et al. 1999a). In the case of GRB 990510, no host galaxy has been detected, even with deep imaging (Israel et al. 1999; Fruchter et al. 1999a). However, the production of a typical afterglow for the interstellar interaction case probably requires that the burst take place in or near a galaxy for the surrounding density to be sufficiently high. For GRB 970508, which we have identified as a wind interactor, the burst is within 0".01, or 70 pc of the galaxy center (Fruchter et al. 1999c). Wind interaction implies a massive star progenitor and the source may have been in a nuclear starburst region. In the case of GRB 970228, the source is about 0".5 from the galaxy center (Sahu et al. 1997), which is comparable to the interstellar interaction case of GRB 990123. Location does not appear to provide a clear discriminator for the two types of bursts considered here.

We have argued that there are two types of burst progenitors, so the GRBs associated with the two types might be expected to have distinct properties. We have examined the data on the GRBs themselves and have found no clear distinction between those that give rise to wind or to ISM type afterglows. In both cases, the γ-ray light curves are complex and last for tens of seconds. One implication is that the mechanism giving rise to the initial GRBs does not depend on the external medium. This supports the generally favored internal shock model for the GRBs (e.g., Piran 1999).

Another implication is that, for both types, the source must be capable of producing a long-duration burst. This is expected for a massive star origin because the collapse time of the stellar core is on the order of tens of seconds (MacFadyen & Woosley 1999; Fryer, Woosley, & Hartmann 1999a). Among the compact binary mergers that have been proposed (Fryer et al. 1999a, and references therein), the type that may satisfy the duration requirement is the black hole–white dwarf merger (Fryer et al. 1999b). In addition, this type of merger is expected to occur in or near the host galaxy, again in accord with observations. For the small number of sources we have discussed here, the rate of massive star explosions is not very different from the rate of compact star explosions. However, the observed interstellar interactors are somewhat more distant and luminous than the wind interactors on average, and the occurrence of GRB 980425/SN 1998bw indicates the presence of low-energy wind interactors. This would imply a higher rate of massive star explosions per unit volume than of compact star explosions. However, if jet effects are more important for interstellar interactors (as suggested by Table 1), the rate of interstellar interactors is increased, so no clear conclusions are possible for the relative rates.

One of the unexpected results of this study is the possible evidence for a relation between jet effects and the afterglow (and thus progenitor) type. Based on a small number of objects, the interstellar interactors show evidence for significant jet effects, while the wind interactors with massive star progenitors do not. This suggests the intriguing possibility that the GRB engine generates a collimated flow, but in the case of a massive star progenitor the flow becomes uncollimated upon passing through the star.

6. CONCLUSIONS

The results of our work can be summarized as follows.

1. The afterglow light curves resulting from the interaction of a GRB with a circumstellar wind have properties that depend on the observation frequency. At radio frequencies, there are two possibilities. Above ν_{Am} (eq. [23]) the light curve is of type D (Fig. 1), and below ν_{Am} it is of type E. Detailed integrations over a spherical blast wave show these segments but without sharp transitions. At high frequencies (optical and X-ray), the expected light curve is of type A (Fig. 1). The evolution may make a transition from cooling ($F_\nu \propto \nu^{-p/2} t^{-(3p-2)/4}$) to adiabatic ($F_\nu \propto \nu^{-(p-1)/2} t^{-(3p-1)/4}$) evolution or may remain in one of these phases during the period of observation depending on the parameters, especially ϵ_B. The transition occurs earlier at lower frequency. For typical parameters, the fast cooling phase (all electrons cool) lasts for $\sim$1–2 days, considerably longer than in the interstellar interaction case. The light curve can be modified from the above expressions during this early phase.

2. During wind interaction, the transition to nonrelativistic evolution occurs at $\sim$2 yr for typical parameters. This is longer than in the interstellar interaction case because of the low density in the outer parts of the wind.

3. The optical synchrotron emission from the early reverse-shock wave has a peak magnitude of $\sim$12 for standard parameters. It could be comparable to the prompt emission for the interstellar interaction case. Radio emission is strongly self-absorbed during this phase.

4. The recognition of supernova emission in the optical radiation from GRB 970228 (Reichart 1999; Galama et al. 2000) implies that the decline of the nonthermal afterglow is faster than previously thought and is compatible with adiabatic wind interaction.

5. The optical spectrum and decline over days 2–100 of GRB 970508 suggest cooling evolution and are compatible with either interstellar or wind interaction models. However, the extensive radio data on this source strongly suggest wind interaction. In our model, the blast-wave energy is 3×10^{51} ergs and the wind mass-loss rate is $3 \times 10^{-6} M_\odot \text{ yr}^{-1}$ for a wind velocity of 1000 km s^{-1}.

6. In the case of GRB 990123, the afterglow showed a steeper decline with time in X-rays than in optical emission, as expected for interaction with a constant-density medium. A prompt optical flash was observed from this object, which can be plausibly attributed to synchrotron emission from the reverse-shock front due to interaction with the interstellar medium (Sari & Piran 1999a, 1999b). We have found that interaction with a wind cannot produce the temporal behavior of the observed flash. The case for interstellar interaction appears to be strong. We have also identified GRB 990510 as a likely interstellar interactor based on its early time evolution.

7. Among the seven sources for which we have suggested identifications, five are wind interactors and two are interstellar interactors, although two of the wind cases can also be interpreted as jets in either a wind or the interstellar medium. The interstellar interactors are somewhat more luminous and distant but appear to have more significant

jet effects, so no clear conclusions can be drawn regarding the relative rates of the two types. However, there does not appear to be a clear distinction in the initial γ-ray burst properties of these different types. This provides additional evidence for a burst model that does not depend on environment, e.g., the internal shock model for bursts.

The main result of our paper is the presentation of evidence for two types of GRB afterglows in different environments: a constant-density interstellar medium and the wind of a Wolf-Rayet star. The types are not immediately distinguishable because, at an age of a few days, the preshock wind density is comparable to an interstellar density. At an age of seconds, the preshock density is higher for the wind case, and we predict that the wind interactors have prompt optical emission that dies off faster than in the interstellar interactors. In addition, we expect the wind interactors to be accompanied by a supernova event. Future observations of GRBs and their afterglows should provide a clear test of our model.

We are especially grateful to the referee, Re'em Sari, for pointing out corrections and for constructive comments in his detailed report. Comments and correspondence from Eli Waxman and Dale Frail were important for clarifying and correcting our model for GRB 970508, although they do not agree with our model. We also thank Andy Fruchter and Pawan Kumar for useful correspondence and conversations. Support for this work was provided in part by NASA grant NAG5-8232.

REFERENCES

Akerlof, C. W., et al. 1999, Nature, 398, 400
Blandford, R. D., & McKee, C. F. 1976, Phys. Fluids, 19, 1130
Bloom, J. S. 1999, talk at Fifth Huntsville Symposium on Gamma-Ray Bursts
Bloom, J. S., et al. 1999a, ApJ, 518, L1
———. 1999b, Nature, 401, 453
Böttcher, M., & Dermer, C. D. 2000, ApJ, 532, 281
Castro-Tirado, A. J., et al. 1999, Science, 283, 2069
Chary, R., et al. 1998, ApJ, 498, L9
Chevalier, R. A., & Li, Z.-Y. 1999, ApJ, 520, L29 (CL)
Costa, E., et al. 1997, Nature, 387, 783
Dai, Z. G., & Lu, T. 1998, MNRAS, 298, 87
Frail, D. A., Kulkarni, S. R., Nicastro, L., Feroci, M., & Taylor, G. B. 1997, Nature, 389, 261
Frail, D. A., Kulkarni, S. R., Shepherd, D. S., & Waxman, E. 1998a, ApJ, 502, L119
Frail, D. A., Waxman, E., & Kulkarni, S. R. 2000a, ApJ, submitted (astro-ph/9910319)
Frail, D. A., et al. 1998b, GCN Circ. 89
———. 2000b, ApJ, 534, 559
Frontera, F., et al. 1998, A&A, 334, L69
———. 2000, ApJS, 127, 59
Fruchter, A. S. 1999, talk at STScI Symposium on The Largest Explosions since the Big Bang: Supernovae and Gamma-Ray Bursts
Fruchter, A. S., et al. 1999a, GCN Circ. 386
———. 1999b, ApJ, 516, 683
———. 1999c, preprint (astro-ph/9903236)
Fryer, C. L., Woosley, S. E., & Hartmann, D. H. 1999a, ApJ, 526, 152
Fryer, C. L., Woosley, S. E., Herant, M., & Davies, M. B. 1999b, ApJ, 520, 650
Galama, T. J., Wijers, R. A. M. J., Bremer, M., Groot, P. J., Strom, R. G., Kouveliotou, C., & van Paradijs, J. 1998a, ApJ, 500, L97
Galama, T. J., et al. 1998b, ApJ, 497, L13
———. 1998c, ApJ, 500, L101
———. 1998d, Nature, 395, 670
———. 1999, Nature, 398, 394
———. 2000, ApJ, in press (astro-ph/9907264)
Ghisellini, G. 1999, preprint (astro-ph/9907376)
Granot, J., Piran, T., & Sari, R. 1999, ApJ, 527, 236
Halpern, J. P., Kemp, J., Piran, T., & Bershady, M. A. 1999, ApJ, 517, L105
Harrison, F. A., et al. 1999, ApJ, 523, L121
Israel, G. L., et al. 1999, A&A, 348, L5
Katz, J. I. 1994, ApJ, 422, 248
Kulkarni, S. R., et al. 1998, Nature, 395, 663
———. 1999, Nature, 398, 389
Li, Z.-Y., & Chevalier, R. A. 1999, ApJ, 526, 716
Livio, M., & Waxman, E. 2000, ApJ, submitted (astro-ph/9911160)
MacFadyen, A., & Woosley, S. E. 1999, ApJ, 524, 262
Mészáros, P., & Rees, M. J. 1997, ApJ, 476, 232
———. 1999, MNRAS, 306, L39
Mészáros, P., Rees, M. J., & Wijers, R. A. M. J. 1998, ApJ, 499, 301
Paczyński, B. 1998, ApJ, 494, L45
Panaitescu, A., & Mészáros, P. 1998, ApJ, 493, L31
———. 1999, ApJ, 526, 707
Panaitescu, A., Mészáros, P., & Rees, M. J. 1998, ApJ, 503, 315
Piran, T. 1999, Phys. Rep., 314, 575
Piro, L., et al. 1998, A&A, 331, L41
———. 1999, ApJ, 514, L73
Reichart, D. E. 1999, ApJ, 521, L111
Rhoads, J. E. 1997, ApJ, 487, L1
———. 1999, ApJ, 527, 737
Sahu, K. C., et al. 1997, Nature, 387, 476
Sari, R. 1997, ApJ, 489, L37
———. 1998, ApJ, 494, L49
Sari, R., & Piran, T. 1995, ApJ, 455, L143
———. 1999a, ApJ, 517, L109
———. 1999b, ApJ, 520, 641
Sari, R., Piran, T., & Halpern, J. P. 1999, ApJ, 519, L17
Sari, R., Piran, T., & Narayan, R. 1998, ApJ, 497, L17
Sedov, L. I. 1959, Similarity and Dimensional Methods in Mechanics (New York: Academic)
Sokolov, V. V., Kopylov, A. I., Zharikov, S. V., Feroci, M., Nicastro, L., & Palazzi, E. 1998, A&A, 334, 117
Stanek, K. Z., Garnavich, P. M., Kaluzny, J., Pych, W., & Thompson, I. 1999, ApJ, 522, L39
Taylor, G. B., Frail, D. A., Kulkarni, S. R., Shepherd, D. S., Feroci, M., & Frontera, F. 1998, ApJ, 502, L115
Vietri, M. 1997, ApJ, 488, L105
Vreeswijk, P., et al. 1999, GCN Circ. 324
Waxman, E. 1997a, ApJ, 485, L5
———. 1997b, ApJ, 489, L33
———. 1997c, ApJ, 491, L19
Waxman, E., Kulkarni, S. R., & Frail, D. A. 1998, ApJ, 497, 288
Wijers, R. A. M. J., & Galama, T. J. 1999, ApJ, 523, 177
Wijers, R. A. M. J., Rees, M. J., & Mészáros, P. 1997, MNRAS, 288, L51
Woosley, S. E. 1993, ApJ, 405, 273